TÉCNICO LISBOA

Computational study of contact patterns in the ankle joint after ligamentous injury

Gonçalo Ribeiro Lopes Rodrigues Marta

Thesis to obtain the Master of Science Degree in

Biomedical Engineering

Supervisors: Prof. João Orlando Marques Gameiro Folgado
Dr. Francisco Guerra-Pinto

Examination Committee

Chairperson: Prof. Patrícia Margarida Piedade Figueiredo
Supervisor: Prof. João Orlando Marques Gameiro Folgado
Members of the Committee: Dr. André Paulo Galvão de Castro
Dr. Bruno José Silva Pereira

November 2018

Acknowledgments

Em primeiro lugar gostaria de agradecer aos meus orientadores, Prof. João Folgado, Prof. Carlos Quental e Dr. Francisco Guerra-Pinto, que durante todos estes meses difíceis me motivaram a querer saber mais, a querer fazer melhor e que nunca me deram o peixe, mas que me ensinaram a pescar.

Um sincero e sentido obrigado aos meus colegas de faculdade que durante estes 5 anos me ajudaram a manter a cabeça no local certo e que comigo partilharam bons e maus momentos. Ao Rafa, Lina, Cate, Manuel, Leitão, Teté, Pipo, Miranda, Dudu, Rodrigo, Bino, Tânia e Ana Carolina, que passaram muito tempo comigo, um agradecimento especial.

Um obrigado especial ao João, à Teresa, ao Rafael, ao Manuel, à Filipa e à Carolina que partilharam o gabinete comigo nestes últimos meses e que me fizeram companhia dia e noite.

Obrigado aos meus amigos que, não estudando no Instituto Superior Técnico, perceberam toda a minha dedicação ao longo destes 5 últimos anos e nunca pensaram duas vezes na altura de estender uma mão em momentos mais duros. À Susana e ao Armando que sempre me incentivaram a correr atrás do que queria (literalmente) e à Joana que sempre foi a minha fã número 1.

À Constança, por me ter abanado na altura certa e da maneira certa. Numa altura onde nada parecia dar certo, não desistiu de mim e puxou-me para cima.

Obrigado à minha família pela possibilidade que me deram nestes últimos 5 anos de trabalhar num dos sítios mais conceituados do mundo e, principalmente, por serem compreensivos e estarem lá para mim mesmo quando a vontade e paciência não eram muitas.

Abstract

The ankle is a complex joint, with the ligaments as its main stabilizer, which when injured, induce instability and a change in the cartilaginous contact pressures. The main goal of this work is to study the changes in those contact pressures as well as the changes in the ligamentous strain and in the ankle reaction moments, using the finite element method (FEM).

This work involved the creation of the finite element (FE) model of the ankle joint (AJ), namely of its mechanical properties and boundary conditions. Three internal rotation (IR) levels, experimentally measured, were applied in the ankle for three different ligamentous configurations.

The results show a high strain rate at the anterior talofibular ligament (ATFL) and at the deep posterior tibiotalar ligament (PTTL), denoting their importance in the ankle's IR. There is also not only an increase of the maximum pressure in the ankle cartilage, but also the occurrence of pressure spots at the anteromedial and posterolateral areas of the talar cartilage, possible precursors of cartilaginous injuries with degenerative implications.

Keywords: Ankle joint; Contact pressures; Ligaments; Finite Element Method.

Resumo

O tornozelo é uma articulação complexa, tendo nos ligamentos os principais estabilizadores que, quando lesionados, induzem instabilidade e uma alteração das pressões de contacto ao nível das cartilagens. O objectivo deste trabalho é estudar as alterações nessas pressões de contacto bem como da deformação ligamentar e do momento de reacção no tornozelo, recorrendo ao método dos elementos finitos.

Este trabalho envolveu a modelação geométrica e do modelo de elementos finitos do tornozelo, nomeadamente das propriedades mecânicas e condições fronteira. Três níveis de rotação interna, medidos experimentalmente, foram aplicados no tornozelo para três configurações ligamentares diferentes.

Os resultados demonstram que existe uma extensão elevada ao nível dos ligamentos talofibular anterior e tibiotalar posterior, denotando a sua importância na rotação interna do tornozelo. Existe, também, não só um aumento da pressão máxima sentida nas cartilagens, como também um aparecimento de pressões ao nível lateral e medial, possíveis precursores de lesões cartilaginosas e com implicações degenerativas.

Keywords: Articulação do tornozelo; Pressões de contacto; Ligamentos; Método de elementos finitos.

Contents

Acknowledgements i

Abstract iii

Resumo v

Index vii

List of Tables ix

List of Figures xi

Acronyms xii

Nomenclature xv

1 Introduction 1
- 1.1 Motivation . . . 1
- 1.2 Thesis Outline . . . 2

2 Background 3
- 2.1 Terminology . . . 3
  - 2.1.1 Anatomical Reference Position . . . 3
  - 2.1.2 Anatomical Reference Planes and Axes . . . 3
  - 2.1.3 Motion Terminology . . . 4
- 2.2 Anatomy . . . 5
  - 2.2.1 Ankle Joint Complex . . . 6
    - 2.2.1.1 Bones . . . 6
    - 2.2.1.2 Ligaments . . . 7
- 2.3 Axis of Rotation . . . 8
- 2.4 Ankle Injuries, Diagnosis and Treatment . . . 9
- 2.5 Finite Element Ankle Models . . . 11
  - 2.5.1 Novel Aspects of the Work . . . 15

3 Methods 17
- 3.1 Parts . . . 17
- 3.2 FE Modelling . . . 20
  - 3.2.1 Ligament Insertion . . . 20
  - 3.2.2 Material Properties . . . 21
  - 3.2.3 Model Interactions . . . 21

3.2.4 Loads . . . 22
3.2.5 Boundary Conditions . . . 22
3.2.6 Mesh Generation . . . 23
3.2.7 Results Presentation . . . 25

4 Results and Discussion **27**
4.1 Model Validation . . . 27
4.2 Cartilage Pressure . . . 28
4.2.1 Results . . . 28
4.2.2 Discussion . . . 30
4.3 Ligamentous Strains . . . 32
4.3.1 Results . . . 32
4.3.2 Discussion . . . 32
4.4 Reaction Moments . . . 33
4.4.1 Results . . . 33
4.4.2 Discussion . . . 34

5 Conclusion **37**
5.1 Limitations and Future Work . . . 38

References **40**

A Appendix A **47**

List of Tables

2.1 Values for the rotation around the three main axes for plantar flexion (PF) and dorsiflexion (DF) in the work done by Lundberg et al.. The values show that for DF and PF, the rotation does not happen only along the transverse axis, but there is also rotation along the other two axes. 9

3.1 Mechanical properties for all the ligaments considered in this work, as well as the cross-sectional areas for each ligament. The material properties were taken from Corazza et al., Liacouras et al., Siegler et al. and Cheung et al.. 22
3.2 Loads and rotations applied for each step in this model. The loads and rotations are negative due to the orientation of the local coordinate system. 23

4.1 Values for the maximum pressure (MPA) on the fibular, tibial and talar cartilages for IRs of 3.67°, 9.6°and 13.43°. 30
4.2 Peak stresses for the talar cartilage of the FE model for IRs of 3.67°, 9.6°and 13.43°and the peak stresses of the ankle joint taken from the work of Wagner et al., Steffensmeier et al., and Calhoun et al. and gathered by Brand. 32
4.3 Strains calculated for 5 ligaments - deep anterior tibiotalar ligament (ATTL), PTTL, posterior talofibular ligament (PTFL), calcaneofibular ligament (CFL) and ATFL - for the 3 degrees of rotation used in this work. Negative strains represent a shortening of the ligament whereas positive ones represent a stretching. The ATFL has been excluded from the 9.6% and 13.43% rotations and the CFL from the 13.43%, having no strains for that reason. 32
4.4 Values for the reaction moments (N m) taken from the FE model for the 3 rotation angles and for 3 different ligamentous configurations. Inside brackets are the normalized values by the reaction moment of the foot with intact ligaments and IR angle of 3.64° 33

A.1 Equivalent stresses for the talar tilt test for a normal ankle and after 3 different lateral collateral ligaments (LCL) reconstruction techniques. Retrieved from Wang et al. 48
A.2 Equivalent stresses for the anterior drawer test for a normal ankle and after 3 different LCL reconstruction techniques. Retrieved from Wang et al. 48
A.3 Values of maximum pressure (MPa) for the 7 cases analyzed by Kimizuka et al [1] and for the FE analysis. 48

List of Figures

2.1 (a) Ankle figure with the three reference planes (b) foot figure with the three reference axis highlighted. . . . 4
2.2 Example of the movements around the three reference axis. . . . 4
2.3 (a) Pronation and (b) supination of the foot. . . . 5
2.4 (a) Anterior view of the distal part of the leg and of the foot (b) superior view of the foot. . . . 7
2.5 (a) Lateral view of the ankle and (b) medial view of the ankle with the lateral and medial collateral ligaments highlighted. . . . 8
2.6 Tests for ligament injury evaluation. (a) Anterior Drawer Test and (b) Talar Tilt. . . . 11
2.7 (a) Ankle model developed by Patil et al. and (b) 3-D ankle model created by Jacob et al.. 12
2.8 (a) Bony structure of the model created by Cheung et al. and (b) FE model of the soft tissue capsule. . . . 12
2.9 FE model built by Ozen et al with the bony structures at the left - and the prosthetic component highlighted with a yellow circle - and the soft tissue capsule at the right. The concrete-like platform can also be seen in orange. . . . 13
2.10 Maximum strains for the ATFL, CFL and PTFL, considering the movements of inversion, inversion plus PF, inversion plus internal rotation and a combination of inversion, internal rotation and PF. Adapted from Wei et al.. . . . 14
2.11 (a) Lateral image of the ankle model used to simulate the anterior drawer test - displacement direction is in yellow (b) frontal image of the ankle model with the red arrows representing the forces applied in the talar tilt test. Adapted from Wang et al.. . . . 15

3.1 Axial view of the evolution of the active contour method of the calcaneus bone for (a) t=0, (b) t=50, (c) t=100, (d) t=150 and sagital view of the 3D evolution of the active contour method of the calcaneus bone for (e) t=0, (f) t=50, (g) t=100, (h) t=150. . . . 18
3.2 Final segmentation of the tibia, fibula and talus after active contour and manual segmentation methods. . . . 18
3.3 (a) Imported talus model from ITK-SNAP and (b) talus model after the Laplacian filtering. 19
3.4 Final model of the foot imported into ABAQUS®, with the bones in grey and the cartilages in red. (a) frontal view of the model and (b) lateral view of the model. . . . 19
3.5 The average and standard deviation of critical parameters . . . 20
3.6 (a) frontal image and (b) lateral image of FE model of the ankle with the main axis (MA) and the coordinate system highlighted in yellow. . . . 23
3.7 Values for the maximum pressure felt on the talar cartilage (MPa) depending on the mesh size (mm) for a compressive force of 650 N. . . . 24
3.8 (a) Ankle meshed FE model; (b) tetrahedral FE mesh of the tibia and fibula and hexahedral FE mesh of the tibial and fibular cartilage; (c) superior view of the hexahedral FE mesh of the talar cartilage. . . . 24

4.1 Plot of the 7 different cases' maximum pressures measured in the talar cartilage from the study of Kimizuka et al in different colors and the FE method values in grey. 27
4.2 (a) FE model of the talar cartilage with the contact pressure values for the 1500 N compressive load. The maximum contact pressure is in red and corresponds to 9.637 MPa and the medial and posterior orientations are marked with a "M"and "P"respectively. (b) *In vivo* pattern of pressure distribution taken from the work done by Kimizuka et al. 28
4.3 Contact pressure (MPa) in the (a) superior surface of the talar cartilage and in the (b) inferior surface of the tibial cartilage for an internal rotation (IR) of 3.67°with (d) being the scale in MPa. M, L and P stand for medial, lateral and posterior orientations respectively. 29
4.4 Contact pressure (MPa) in the (a) superior surface of the talar cartilage in the (b) inferior surface of the tibial cartilage and in the (c) medial surface of the fibular cartilage, for an IR of 9.6°with (d) being the scale in MPa. M, L, P and S stand for medial, lateral, posterior and superior orientations respectively. 29
4.5 Contact pressure (MPa) in the (a) superior surface of the talar cartilage in the (b) inferior surface of the tibial cartilage and in the (c) medial surface of the fibular cartilage, for an IR of 13.43°with (d) being the scale in MPa. M, L, P and S stand for medial, lateral, posterior and superior orientations respectively. 30
4.6 Values for the normalized reaction moments in the foot, for IRs of 3.64°, 9.6°and 13.43°and for the model with intact ligaments - blue trace - with ATFL cut - orange trace - and ATFL and CFL cut - green line. 34

A.1 Acute ankle injury diagnosis algorithm. 47
A.2 (a) FE model of the talar cartilage with the contact pressure values for the 500 N compressive load. The maximum contact pressure is in red and corresponds to 6.239 MPa and the medial and posterior orientations are marked with a "M"and "P"respectively. (b) *In vivo* pattern of pressure distribution taken from the work done by Kimizuka et al [1]. . . 49
A.3 (a) FE model of the talar cartilage with the contact pressure values for the 1000 N compressive load. The maximum contact pressure is in red and corresponds to 7.865 MPa and the medial and posterior orientations are marked with a "M"and "P"respectively. (b) *In vivo* pattern of pressure distribution taken from the work done by Kimizuka et al [1]. . . 49

Acronyms

AJ ankle joint.

AJC ankle joint complex.

AS ankle sprain.

ATFL anterior talofibular ligament.

ATiFL anterior tibiofibular ligament.

ATTL deep anterior tibiotalar ligament.

CaCL calcaneocuboid ligament.

CFL calcaneofibular ligament.

CI chronic instability.

CNL calcaneonavicular ligament.

CuNL cuboideonavicular ligament.

DF dorsiflexion.

FE finite element.

FEM finite element method.

IR internal rotation.

LCL lateral collateral ligaments.

MA main axis.

MCL medial collateral ligaments.

MI mechanical instability.

OA osteoarthritis.

PF plantar flexion.

PTFL posterior talofibular ligament.

PTiFL posterior tibiofibular ligament.

PTTL deep posterior tibiotalar ligament.

RA rheumatoid arthritis.

STTL superficial tibiotalar ligament.

TaFi talofibular.

TC talocrural.

TCN talocalcanealnavicular.

TiCL tibiocalcaneal ligament.

TiFi tibiofibular.

TiNL tibionavicular ligament.

TSL tibiospring ligament.

TT tibiotalar.

Nomenclature

E	Young's Modulus
ν	Poisson's Ratio
ε	Cauchy Strain
k	Spring's Constant

Chapter 1

Introduction

This is an introductory chapter, in which the motivation for this work is described, the objectives are set and a description of the organization of the thesis is done.

1.1 Motivation

The AJ is a very complex system composed of three individual joints: the tibiotalar (TT), the talofibular (TaFi) and the tibiofibular (TiFi), acting as a link between the leg and the foot. Both the anatomical and biomechanical characteristics of the ankle joint allow it to be a major weight-bearer in all of the daily activities, transferring the loads between the leg and the foot. This characteristic is highly important since the foot is the basis used by the body to stand, walk and run and the loads generated in these activities are all partially supported by the AJ [2].

The complexity of the AJ and the large forces applied in the legs and feet lead to a high incidence of injuries, with ankle sprain (AS) and arthritis being the ones with the higher occurrence rate. In fact in a study made by Yung et al., ankle injuries are ranked the most popular injured body site with 34.3% of all injuries, followed by knee injuries. Among ankle injuries, ankle sprains are the most common [3].

An AS happens when ligaments supporting the ankle stretch beyond their limits and tear with 3 possible severity degrees [4]. The diagnosis and injury quantification for AS, however, depend highly on the mobilization made by the orthopedist, which is very subjective [5].

Arthritis is a pathology that disrupts the normal function of joints by destroying their articular surface. The two forms of arthritis that are most common are osteoarthritis (OA) and rheumatoid arthritis (RA) [6]. OA develops in joints that are injured or that are repeatedly overused, wearing the cartilage at the end of the bones. If the cartilage damage occurs after trauma it is called secondary OA [6]. On the other side, RA is an autoimmune inflammatory disease, in which the body releases a group of enzymes that destroy the cartilage of joints [7]. Many authors establish a correlation between ligamentous injuries and a progressive degenerative arthritis of the ankle joint [8, 9]. Taga et al.[10] examined arthroscopically both stable and unstable ankles, and observed that for stable ankles - or ankles that underwent any kind of ligamentous reconstruction after LCL injury - the cartilage damage was not as proeminent as the damage observed in unstable ankles, which had high wear rates especially in the medial side of the tibial and talar cartilage. An association between LCL injury and cartilage lesion was then established.

The main goal of this work is to simulate IR of the ankle for 3 different ligamentous configurations - based on the work done by Guerra-Pinto et al. [5], in which the ankle rotational instability is tested after the cut of successive LCL - and extract not only the strain felt by each ligament during the rotation but also the cartilage pressure in the ankle cartilages and the reaction moments applied on the model. For this purpose, a FE model of the AJ, with appropriate mechanical properties and boundary conditions is

developed.

1.2 Thesis Outline

This thesis is divided into 5 chapters. The first chapter includes a brief introduction and motivation for this work and its objectives.

In chapter 2, the anatomical and biomechanical characteristics of the AJ are described, as well as the injury mechanisms and consequent diagnosis and treatment processes. Also in this chapter, a description of the previous work in FE ankle models is done, highlighting the most important breakthroughs that represent the basis of the model developed here.

Chapter 3 describes all the detailed methodology and computational work, including the modeling of the ankle components and the development of the FE model - material properties, interactions, loads and boundary conditions. The mesh generation is also described in this chapter along with a convergence study to support the choice of mesh size.

Chapter 4 includes a model validation, where the results for a compression analysis are presented and compared with the literature. This chapter comprises also the results for the simulations, being analyzed in the first place the contact pressures in the cartilage, in the second place the ligamentous strains and lastly the reaction moments of the AJ. The discussion of the obtained results is also done in this chapter, describing then the strengths and limitations of this work.

Chapter 5 is the last chapter and includes not only the main conclusions of the work developed, but also suggestions for future work.

Chapter 2

Background

In this chapter, the anatomical and biomechanical characteristics of the ankle joint (AJ) are described, along with the injury mechanisms and consequent diagnosis and treatment processes. Then, a detailed description of the previous work in finite elements (FE) ankle models is done.

2.1 Terminology

To describe the systems under study, precise terminology should be used to identify flawlessly, not only the position but also the direction of the structures. The anatomical reference position was then created and all the planes, axes and motions are defined after this position.

2.1.1 Anatomical Reference Position

The anatomical reference position is only a conventional position, where the body is in a erect standing position with the feet slightly separated, the arms to the side with the palms of the hands facing forward [11]. Directional terms are then defined after this position, with superior being closer to the head and inferior farther from it, anterior towards the ventral side and posterior to the dorsal side, medial as being close to the midline of the body and lateral away from it, proximal as being closer to the trunk and distal away from it and, lastly, superficial as being towards the body surface and deep as being away from it [11].

2.1.2 Anatomical Reference Planes and Axes

From the anatomical reference position, three main planes can be described. The coronal plane, which divides the body into its anterior and posterior parts, the sagittal plane, dividing it into left and right halves and the axial - or transverse - plane, which divides the body into superior and inferior parts. All these planes intersect at a single point when the body is in the anatomical reference position: the center of gravity, or the body's center of mass [11].

To each plane of movement corresponds an axis, which is perpendicular to it: the mediolateral axis, perpendicular to the sagittal plane, the anteroposterior axis, perpendicular to the coronal plane and the longitudinal axis, which is perpendicular to the transverse plane. Consequently, the rotation in the three planes, coronal, sagittal and axial occurs around the anteroposterior, mediolateral and longitudinal axis respectively. All these planes and axes are illustrated in Figure 2.1 [11, 12].

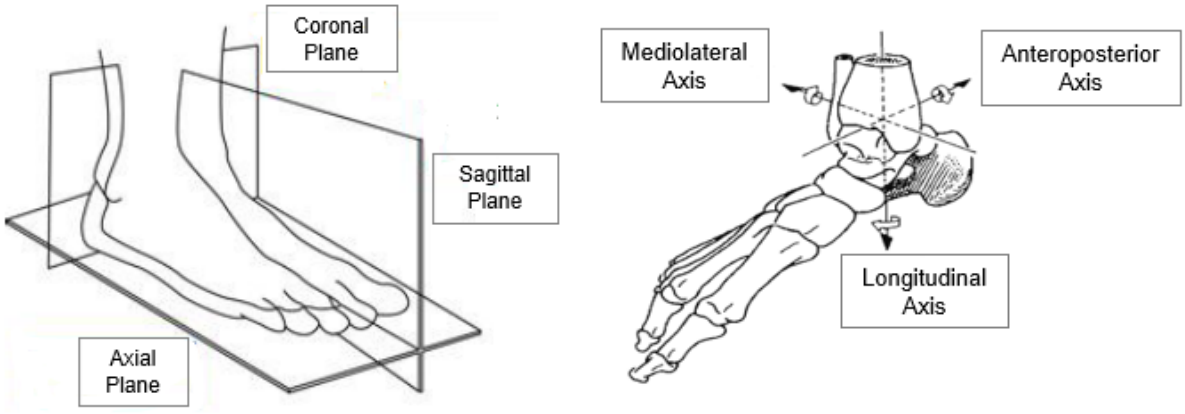

Figure 2.1: (a) Ankle figure with the three reference planes (b) foot figure with the three reference axes highlighted. Adapted from [11, 12].

2.1.3 Motion Terminology

The bulk of human motion consists in a combination of linear and angular motion - both of these being pure forms of motion. Complex movements can be broken down into their linear and angular components for analysis [11]. In the human anatomical reference position, all body segments are considered to be at zero degrees of rotation. Due to this, the measurement of any amount of rotation is done by measuring the angle between the final position of the member and the initial reference position. Also, the movements are named after the direction of motion in relation to the anatomical reference position [11]. Namely, in the ankle, it is possible to identify a set of movements around the axis mentioned above - and, consequently, in the three anatomical planes. In the sagittal plane there are dorsiflexion(DF) and plantarflexion(PF), where the first occurs when the toes are brought towards the lower leg and the latter when they are driven away from the lower leg, being pushed towards the ground.

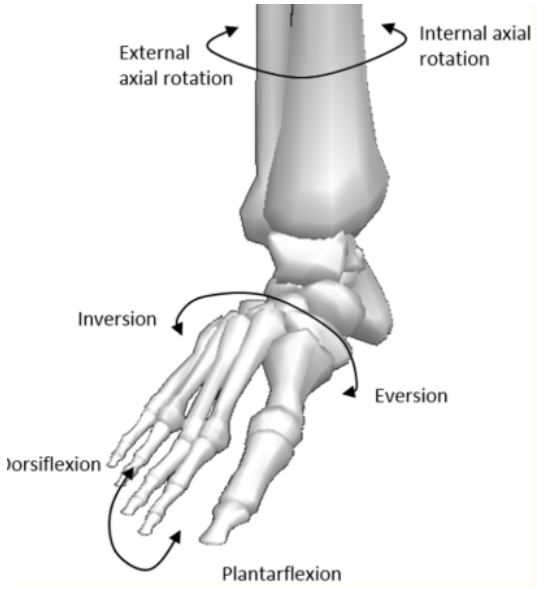

Figure 2.2: Example of the movements around the three reference axis. Adapted from [13]

In the coronal plane take place eversion and inversion. The first rotates the sole of the foot to the lateral side while the second rotates the foot medially. The last set of movements are abduction and

adduction - or external and internal rotation (IR) respectively - and occur in the axial plane. Abduction is defined as the motion of bringing the distal part of the foot away from the medial line of the body and adduction as the motion of bringing the same distal part of the foot towards the medial line of the body [11, 12, 14]. The motions described can be seen in detail in figure 2.2.

Using a combination of all the foot movements described, two more movements can be described, pronation and supination, which can be seen in figure 2.3. Pronation consists on a combination of eversion of the heel, abduction of the forefoot and DF of the subtalar and midtarsal joints whereas supination comprises the movements of inversion, adduction and PF of the corresponding joints of the pronation [15].

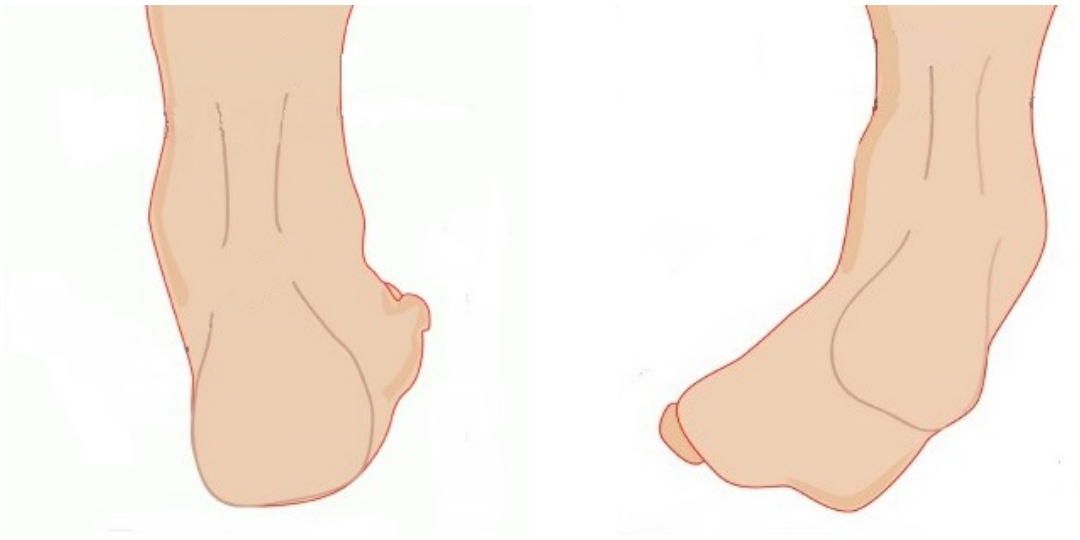

(a) (b)

Figure 2.3: (a) Pronation of the foot and (b) supination of the foot. Adapted from [16].

2.2 Anatomy

Bone, along with ligaments and cartilage, comprise 20% of the human body weight. Bone, particularly, is of extreme importance due to several basic functions performed by it, namely the support to soft tissues and attachment points to tendons of some skeletal muscles, protection of internal organs such as the brain, the spinal cord and the heart and lungs, and mineral homeostasis as stores minerals such as calcium and phosphorus [14].

Cartilage is an avascular form of connective tissue that not only supports soft tissues, but also acts as a gliding surface for bone articulations at joints and allows for the development and growth of long bones in a early stage of life. In this work, only one type of cartilage will be considered - hyaline. Hyaline cartilage is the most common where the matrix contains a moderate amount of collagen fibers [17]. The response of cartilage to stress is unique due to a specific composition and structural organization [18]. However, with injury, there are reports of changes in the collagen network causing a softening of cartilage, extending the degenerative changes into deeper cartilaginous zones [19]. These changes can hardly be reversed since cartilage lacks a regenerative capacity [20].

Ligaments are dense parallel fibers of connective tissue that hold bones close together in what are called joints [14]. Joints can be divided into synovial, fibrous or cartilaginous, depending on the configuration. Synovial joints have a joint capsule with an inner synovial membrane and an external fibrous membrane. The articular lubrication is ensured by the synovial fluid - produced by the synovial

membrane. Fibrous joints do not have a synovial cavity, but rather are composed of dense irregular connective tissue. Cartilaginous joints occur when the bones are held together by cartilage [14].

2.2.1 Ankle Joint Complex

The human ankle joint complex (AJC) comprises a set of different joints. However, not all of them possess the same range of motion [17], thus having different functions on the foot movement. Two main joints can be described in this area: The talocrural (TC) joint (or commonly called ankle joint) and the talocalcanealnavicular (TCN) joint or lower ankle joint [21]. Some authors do not consider the TCN joint as a whole, but separate it into talocalcaneal and calcaneonavicular [17, 14]. However, for the simplicity of the description, all the three bones will be considered in the TCN joint. The TC joint is formed between the distal parts of the tibia and the fibula and the talar dome, while the TCN joint includes the calcaneus, the talus and the navicular bone [17, 22].

Other existing joints include the calcaneocuboid joint, formed by the calcaneus and the cuboid bones, the distal tibiofibular joint, formed by the distal portions of the tibia and the fibula and the tarsometatarsal joints, between the metatarsal bones and the adjacent tarsal bones [17]. These, however, allow only for small movements and will not be considered in this work.

All of these joints are surrounded by a large group of collateral and syndesmotic ligaments, tendons, muscles, nerves, veins and arteries [23]

2.2.1.1 Bones

The lower limb comprises the thigh, the leg and the foot, but only bones from the leg and foot take part in the AJ and these are classified depending on their shape. Long bones are tubular and short bones, the majority of the foot bones, are cuboidal [17]. The tibia and the fibula are the only foot bones classified as long. Figure 2.4 presents both an anterior and superior view of the foot and distal portion of the leg.

The tibia is the weightbearing bone of the leg. It is situated on the medial side of the leg and connects to the fibula through the interosseus membrane [17, 23]. As every long bone, the tibia has a body and two extremities. The upper extremity takes part in the formation of the knee joint and the lower extremity in the formation of the ankle joint. The distal part of the tibia prolongs downwards on the medial side as a proeminence called the medial *malleolus* [23, 24].

The fibula is also a long bone, parallel and lateral to the tibia, although being smaller and not participating in weightbearing. It articulates proximally with the lateral condyle of the tibia and distally, through an arrowed-shape projection called lateral *malleolus*, with the talus and the tibia, forming the AJ [14].

The talus, or astragulus, is the most proximal bone of the foot and interacts directly with the leg bones [17]. It is composed of three parts, these being the body, the neck and the head. One of the main characteristics of the talus is the existence of a lateral process which articulates directly with the fibula [14]. It is of major importance during the gait cycle since it transmits almost half of the weight of the body to the calcaneus and the remainder of it to the other tarsal bones [14].

Distal to the talus is the calcaneus, which is the strongest and largest tarsal bone. It projects behind the ankle joint to form the heel, while articulating proximally with the talus and anteriorly with the cuboid. It is the main responsible for the transmission of the weight of the body to the ground [17, 25, 26]

The navicular bone situates on the medial side of the foot and was given this name due to the boat shape that it takes. It articulates posteriorly with the talus and anteriorly with a group of bones, namely the cuboid and the cuneiforms. It has a tuberosity which accommodates the insertion of the tibialis posterior tendon [17].

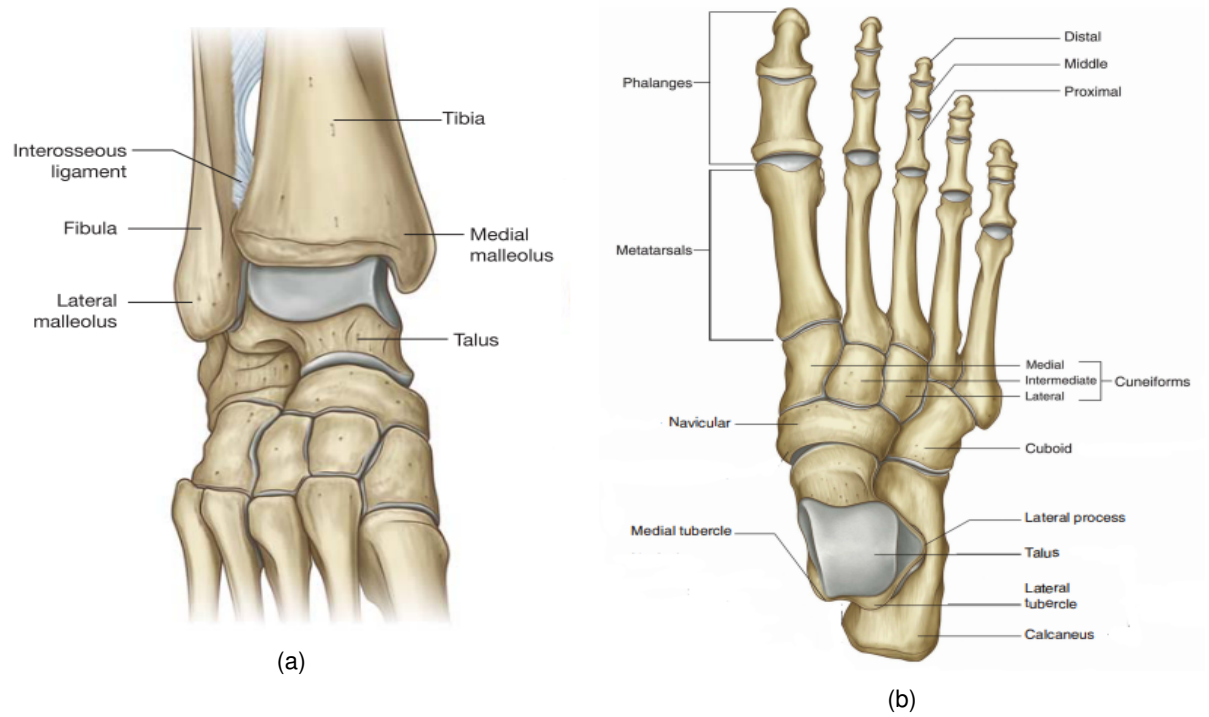

Figure 2.4: (a) Anterior view of the distal part of the leg and of the foot (b) superior view of the foot. Adapted from [17].

Distally to the calcaneus, talus and navicular, set the cuboid and three cuneiforms, which articulate with the five metatarsals. These create a transverse arch high medially and low laterally [23].

The last set of bones is the phalanges, comprising the distal component of the foot and mirroring those of the hand. They represent the bones of the toes and each toe has three phalanges - proximal, middle and distal phalange - except for the thumb, which only has proximal and distal phalange [17].

2.2.1.2 Ligaments

The AJC ligaments enable the ankle to function with a high degree of stability [13]. However, not every ligament has the same relevance, being possible to highlight 3 ligamentar complexes that are of major relevance for this work and for the overall stability of the AJC: the lateral collateral ligaments (LCL), the medial collateral ligaments (MCL) - also known as deltoid ligament - and the syndesmotic ligament complex [13]. Figure 2.5 illustrates both a lateral and medial view of the ankle, focusing on the lateral and medial ligaments.

The lateral collateral ligaments are composed of the ATFL, the PTFL and the CFL. The description of the medial collateral ligaments, however, varies largely in the literature. The most widely accepted description is the one from Milner et al., who studied the collateral ligaments from 40 ankles of 20 cadavers and described the lateral ligaments as being divided into a main group of bands, including the tibiospring ligament (TSL), the tibionavicular ligament (TiNL) and the PTTL, and a secondary group of bands such as the tibiocalcaneal ligament (TiCL), the superficial tibiotalar ligament (STTL) and the ATTL.

Lastly the syndesmotic complex, which is not a synovial articulating joint, is composed of the anterior tibiofibular ligament (ATiFL), the posterior tibiofibular ligament (PTiFL) and the interosseus membrane - a band of fibrous tissue[13].

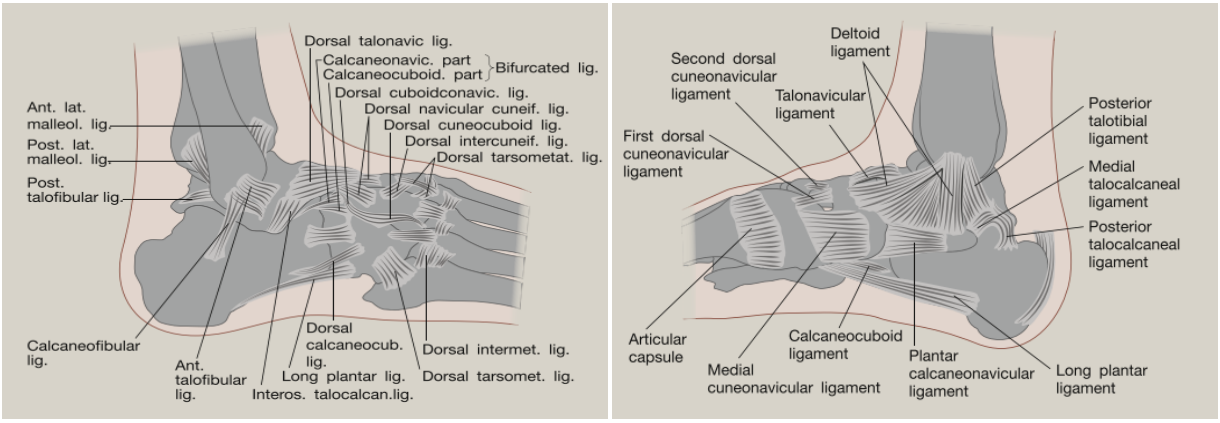

(a) (b)

Figure 2.5: (a) Lateral view of the ankle and (b) medial view of the ankle with the lateral and medial collateral ligaments highlighted. Adapted from [13]

2.3 Axis of Rotation

By not consisting of a single joint, the ankle has a rather complex and dynamic nature [27]. Accordingly, there are still some doubts when the subject is the axis of rotation of the ankle joint. According to Singh et al.[28], the disparity between the ankle motion theories derives from a perspective error.

Goodsir [29] stated in 1859 that the TC joint only had a single axis, which passed through the center of the talar body, while Fick [30], almost fifty years later, proposed a new variable axis, with a changing position dependent of the joint movement. Both of their works were verified by Isman et al.[31] and Sammarco et al.[32] respectively. Isman et al. [31] used cadaveric legs with their ligaments and capsular structures intact to determine the location of the TC axis of rotation with respect to some anatomical marks of the leg. They concluded that the axis of rotation was distal to the tips of the tibial and fibular malleoli. Through the evaluation of instant centers of rotation of the talus using roentgenograms, Sammarco et al. [32] claimed that, due to the imperfect geometry of the talar dome, the instant centers of rotation of the TC joint were constantly changing and that the motion from that joint was not isolated from the TCN joint. Moreover, this change was especially seen in both forced DF and PF due to the gliding and compression associated.

Before Sammarco et al. [32] postulated the moving centers of rotation, Barnett et al. [33] examined more than one hundred and fifty tali and hypothesized about the possibility of the TC joint having two different rotation axes - one for PF, inclined downwards and medially, and one for DF, inclined also downwards but laterally. This happened due to the different medial and lateral radii of curvature and due to the wedged talar shape, which could not preserve the congruency of movement through the sagittal plane. Furthermore, not only the change in the axis was proven to be abrupt from the neutral position to both DF and PF - not being gradual -, but also the axis was found to be roughly horizontal in the neutral position of the ankle. Hicks [34] confirmed in 1953 the existence of a moving axes of rotation for DF and PF, findings later confirmed by Lundberg [35, 36, 37, 38], who postulated the existence of two different axes also for DF and PF, which changed throughout the movement. The existence of these axes is linked to the participation of other joints distal to the talus, causing, along with other extra movements, an internal or external rotation around the longitudinal axis and a supinatory rotation around the anteroposterior axis. The results for this experience, confirming the multiaxial rotation in PF and DF, are shown in table 2.1. The angles were given as differences compared with the neutral postion, where positive values denote plantar flexion, IR and supination around the mediolateral, longitudinal and anteroposterior axes respectively. Lundberg also found, as Isman did, that if he projected the flexion axis

of the ankle onto the horizontal plane, it would ran close to the tips of the lateral and medial malleolus. The main discovery for Lundberg was, however, that when all the axes of PF, DF, pronation, supination, internal and external rotation for the same patient are drawn together, they all run close to one point in the trochlea of the talus. This point is, most likely, the point in the TC around which the ankle has a higher freedom of movement [35]. This is of most importance, especially in prosthetic design.

Table 2.1: Values for the rotation around the three main axis for PF and DF in the work done by Lundberg et al.. Retrieved from [36]. The values show that for DF and PF, the rotation does not happen only along the transverse axis, but there is also rotation along the other two axes.

Input foot position	Rotation (°)		
	Transverse axis (means $\pm$ S.D.)	Vertical axis (means $\pm$ S.D.)	Anteroposterior axis (means $\pm$ S.D.)
Plantarflexion			
30	27.9 $\pm$ 7.7	-0.6 $\pm$ 3.0	-4.3 $\pm$ 1.9
20	20.8 $\pm$ 4.1	0.6 $\pm$ 2.4	-3.7 $\pm$ 1.6
10	11.1 $\pm$ 1.1	1.4 $\pm$ 0.9	-2.2 $\pm$ 0.9
Dorsiflexion			
30	-5.9 $\pm$ 2.3	-1.8 $\pm$ 0.9	0.8 $\pm$ 0.6
20	-15.6 $\pm$ 4.0	-5.6 $\pm$ 1.5	1.4 $\pm$ 1.3
10	-22.7 $\pm$ 3.0	-8.9 $\pm$ 1.9	1.6 $\pm$ 2.0

The disagreement about the position of the axis of the TC joint still lingers in the scientific community, despite the new approaches with mathematical models and new techniques to track small motions in both DF and PF. On one side, in 1992, Singh et al. [28] were able to verify a single DF/PF axis using MRI and photographs of the AJ with LEDs attached. It is commonly accepted that the single flexion-extension axis was shown to lie just distal to the tips of both malleoli. Just two years after Singh, Bogert et al.[39] created a mathematical model with the premise that the TC joint was an ideal hinge joint with a single DF/PF axis. The model started with an initial guess of 12 intrinsic parameters and was later adjusted using kinematic data from 14 male volunteers. The results are close to the ones documented by Isman et al..

On the other side, Thoma et al. [40] in 1993 used mathematical procedures to predict the ankle principles, verifying that the single-axis hinge model for the TC joint did not match the curve that was actually found. The mathematical model was then changed into a model of a link chain with four pivots - implying rotary and gliding components of the tibia against the talus - and there was a much better correlation between the kinematic experimental data and the predictions from the model [40]. The four pivot model was also used later in 1999 by Leardini et al. [41], who reported that the instant center of rotation of the TC joint moved from a postero-inferior to an antero-superior position while the foot went from maximal PF to maximal DF.

To sum up, there is no agreement of the scientific community on the position of the AJ rotation axis, which leads into a wide variety of approaches for diagnosis, treatment and even on the mechanical models that will be discussed further on.

2.4 Ankle Injuries, Diagnosis and Treatment

An ankle sprain (AS) happens when there is a forced movement in the ankle, causing injury to the ligaments. There are some predisposing factors to this type of injury, such as muscular exhaustion, ligamentous laxity and neurological changes including proprioceptive deficit caused by previous trauma. AS can be classified using the severity of the injury [42]. Grade I is described as a mild stretching of the ligaments without rupture and joint instability. Grade II includes a partial rupture of the ligaments

and small to moderate instability. Patients with this grade of injury are reported to have problems with weight bearing. Grade III is a complete ligament rupture that leads to pain, swelling and a high degree of instability [43].

One of the main problems that can arise from successive AS is chronic instability (CI). It is a frequent problem seen in athletes and can be labelled as both mechanical instability (MI) and functional instability (FI). The first one is characterized by the abnormal and excessive ankle movement past the physiological limit of a healthy ankle range of motion (ROM) and the second one is subjective as it is described as a feeling of ankle instability, most likely due to both neuromuscular and proprioceptive deficits [44]. The latter arises due to the hypothesis that an injury to the ligaments also results in damage to the sensory receptors in those ligaments, despite the fact that the proprioceptive mechanisms are yet to be completely clear [44]. Even though muscular weakness is not a major cause of CI, it can be a precursor of ankle injuries [45].

Anatomically, lateral ASs have been described as being more probable than medial sprains mainly due to the talocrural axis of rotation, which is oblique to the long axis of the lower leg, leading to higher tensile forces in the lateral ligaments compared to medial ligaments. These lateral ligaments are also more solicited in daily activities since they prevent not only the anterior displacement of the talus - the talar tilt, but also the excessive inversion and the internal rotation of the talus on the tibia [46]. Medial AS are less common than lateral sprains, due to the strength of the deltoid ligament and due to the lower rupture loads presented by the lateral ligaments - which makes them easier to rupture. In 1877, Hönigschmied [47] was the first one to describe closely the sequence of rupture of the lateral ligaments, followed almost 100 years after by Rasmussen who, in a work developed in 1985, specified the reactions in terms of rotation of the ankle when a forced movement was applied. Rasmussen went even further and described the behavior of the ankle after transection of not only the lateral ligaments, but also the medial ligaments. This work was important to understand and document the ROM of the ankle and the importance of the ligaments in the ankle mobility and stabilization.

The treatment includes surgery for ligament repair, balance training to help stabilize the joint and functional treatment using bandages or tape [43]. Zwipp et al., in 1985-1986 tried to determine the best treatment for ruptured ankle ligaments, comparing surgery combined with immobilization or functional treatment and a conservative approach (without surgery), but the study was inconclusive since all the approaches were equally effective. On one hand, patients who underwent surgery had a slightly better subjective stability than the ones who went through a conservative approach. On the other hand, patients treated conservatively had a better range of active movement due to a higher amount of movement in the earlier stages of the treatment [48].

Hence there seems to be a *status quo* in terms of treatment for ligament rupture. However, the diagnostic is still quite subjective and there are no standardized examination procedures or evidence-based treatments. Moreover, imagiology processes can help on the diagnosis but they represent extra costs [49]. In a study made in 2012, an algorithm for diagnosis and treatment of acute ankle injuries was developed. This algorithm, which is schematically shown in Figure A.1 in the Appendix A, includes both the tests for ankle fractures, namely the Ottawa Rules, and for ankle ligament injuries, which are the anterior drawer test and the talar tilt test.

Both the Ottawa ankle rule and the Ottawa foot rule were developed as a mean to avoid unnecessary X-rays, excluding immediately the possibility for fractures. To perform these tests, certain foot and ankle areas must be examined, such as the tip of the lateral and of the medial malleolus, the base of the fifth metatarsal bone and the navicular bone, and search for bone tenderness. The innability to bear weight for four steps at the emergency department is also a condition that leads to an X-ray [50].

Regarding the tests to evaluate ankle injuries, the anterior drawer test consists in, pressing the heel forward, with the knee joint flexed, while holding the tibia back. This test is used to evaluate the extension

of the injury on the ATFL. On the other hand, the talar tilt is used to assess the injury extension on the CFL and on the ATFL. The test consists on inverting the talus and the calcaneus on the tibia. An example of both of these tests is illustrated in Figure 2.6.

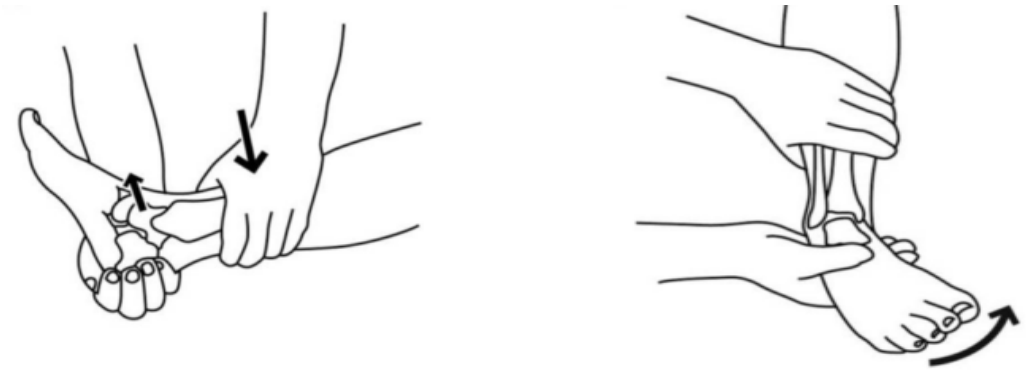

(a) (b)

Figure 2.6: Tests for ligament injury evaluation. (a) Anterior Drawer Test and (b) Talar Tilt. Adapted from [50]

The anterior drawer test is considered as the most important sign of ATFL injury. As documented by van Dijk et al. [49], a rupture of this ligament allows for the rotation of the talus out of the ankle mortis, with the center of rotation being the deltoid ligament. This manoeuver is, nevertheless, associated with a high variability in its sensitivity [5], being the reason why a new approach to the clinical diagnosis needs to be developed. The work from Guerra-Pinto et al. [5], which comes to alter the paradigm for the diagnosis of ligament injury - and is the starting point for this thesis -, is based on the hypothesis that a sequential sectioning of the lateral ligaments of the ankle results in a progressive angular ankle laxity when an internal rotation is applied, resulting in a completely different approach to the diagnosis phase. Guerra-Pinto et al. found that the ankle would increase almost threefold the IR after single ATFL cut and almost fourfold after ATFL and CFL cut. With these findings, they were able to conclude that this evidence of rotational laxity was a major step to define a new diagnostic method for LCL injury, avoiding further inconsistencies and variability in its diagnosis.

2.5 Finite Element Ankle Models

Ankle models started to be developed side by side with the necessity to report the stress patterns of the foot, allowing for a better understanding and prevention, at the time, of some diseases such as diabetes and leprosy. The studies started with Nakamura [51], who developed a 2-D model for the soft tissues of the foot's plantar aspect, including muscles, fascia and skin, as well as a molded foam sole. The objective was to document the stress distribution in the foot, in particular of a diabetic foot. The model, however, did not contemplate bony structures, as they were only included later in 1993 in a work conducted by Patil et al.[52], in which the stresses during three different gait positions - mid-stance, heel strike and push off - were studied.

The model, seen in Figure 2.7, included 2-D representations of the talus and calcaneus bones combined, the navicular bone and the cuneiform and metatarsal bones also combined. The tibia was not used in the simulations. Only two years later, Jacob et al.[53] created a 3-D model of the foot using two different arches. The medial one consisting of the talus, navicular, the three cuneiforms, three metatarsals and three toes, whereas the lateral arch included the calcaneus, the cuboid, two metatarsals and two toes. This model included also the cartilages between the bones and the ligaments, both medial and lateral. However, only simulations for the mid-stance gait phase were done to study the stress

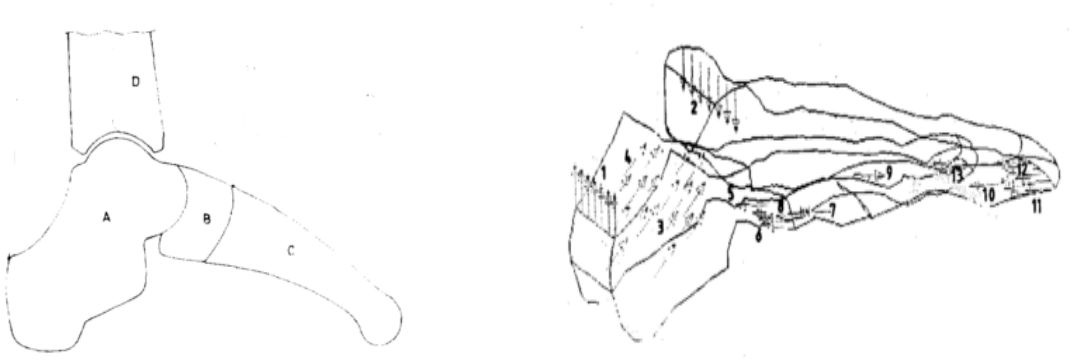

(a) (b)

Figure 2.7: (a) Ankle model developed by Patil et al.. Adapted from [52] (b) 3-D ankle model created by Jacob et al.. Adapted from [53]

regions. The results showed that the ankle joint supports most of the body weight during that period of time.

Despite the constant different approaches developed, the existing foot models still lacked complexity, both on the anatomical point of view - due to the combination of two or three bones - and on the mechanical point of view, since, until then, ligaments and cartilages were modelled using a linear elastic behavior, while in fact they have a non linear behavior [54]. In 2000, Gefen et al. [55] created the first 3-D finite element model of a normal foot structure, including ligaments and cartilage and used it to simulate the joint behaviour of discrete moments of the gait cycle. *In vivo* measurements of the gait cycle using techniques such as contact pressure display method and digital radiograpic fluoroscopy were made to accurately pinpoint the position of the foot as well as the plantar pressure pattern. The model was able to predict, during 6 phases of the gait cycle, the von Mises stresses of the bony structures.

Five years after, Cheung et al. [56] created a 3-D model of the foot contemplating both bony structures and other types of tissue such as ligaments, cartilage and the plantar fascia. The model had also a soft tissue capsule, modeled using an hyperelastic law, which involved all of the other structures. The main goal was to evaluate the plantar pressure and the internal load transfer between bones during standing, being of particular importance for diabetic patients, who often suffer with plantar foot ulcers. Figure 2.8 shows the final model for both the bony structures and the encapsulated soft tissue. This

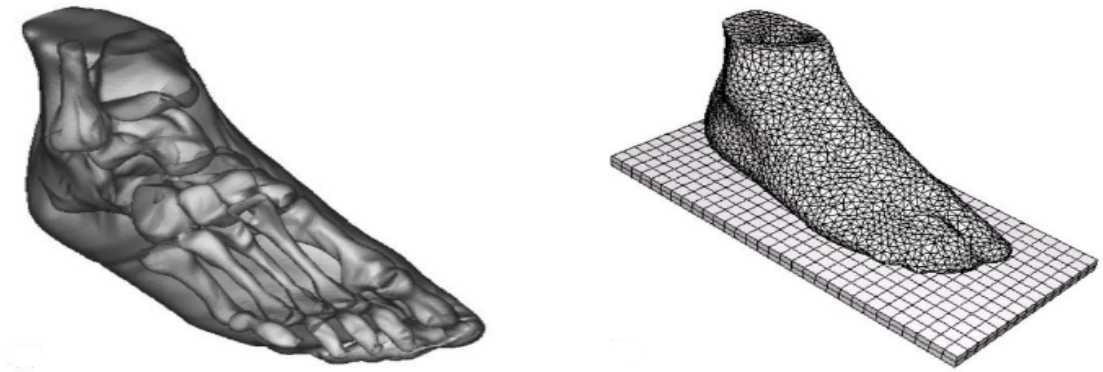

(a) (b)

Figure 2.8: (a) Bony structure of the model created by Cheung et al.. (b) FE model of the soft tissue capsule. Adapted from Cheung et al. [56].

model was able to predict with accuracy plantar stress patterns, which concentrated in the heel and in the medial metatarsal heads areas. The results from this study were in line with the observations of

plantar foot ulcers at the medial forefoot and heel regions of diabetic patients, indicating that the model was robust and could be used for different simulations [56].

Ankle FE models have also been used to predict and study stress patterns in the articular surfaces and in the bones, especially in advanced stages of arthritis, where a total ankle replacement needs to be considered. This is a relatively new concept and, although the existing literature describes a high success rate for this kind of procedure [57, 58], the high costs and difficulties in experimental studies slow the further development of the technique. Because of their flexibility, FE are an attractive alternative that can provide valuable information. In 2013, Ozen et al. [59] studied both the stress patterns and the plantar pressure of a normal foot-ankle complex versus those of a prosthetic foot-ankle complex. The model built was extremely complex, as depicted in Figure 2.9 with a total of 20 bones, 76 ligaments, plantar fascia and a capsule of soft tissue. For the prosthetic components, the Buershel Pappas Total Ankle Replacement system was chosen, consisting on a tibial component, a talar component and an interlaying mobile bearing that resembled the ankle cartilage. A ground support platform modelled after concrete was also included. The model was validated using the plantar pressures available in the literature for a 400N compressive force applied on each foot - considering a subject of 80 kg.

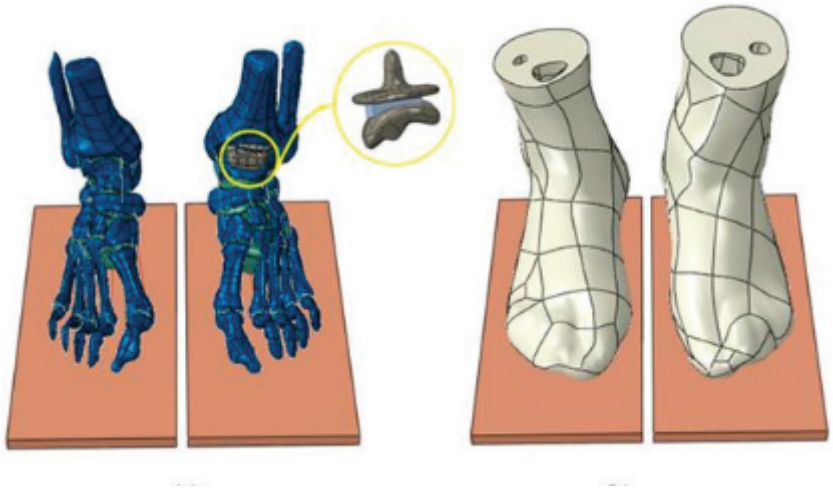

Figure 2.9: FE model built by Ozen et al [59] with the bony structures at the left - and the prosthetic component highlighted with a yellow circle - and the soft tissue capsule at the right. The concrete-like platform can also be seen in orange. Adapted from Ozen et al. [59].

The results for the normal foot stresses were in line with the literature present at the time, having peaks of von Mises stresses at the 2nd and 3rd metatarsal, at the tibia and at the calcaneus. For the prosthetic complex, the peak stresses changed, having a higher von Mises stress at the tibia and 4th and 5th metatarsal bones. Regarding the plantar pressures, the results revealed an expected peak pressure at the heel and forefoot for the normal foot and an even higher peak pressure at the forefoot for the prosthetic foot [59]. Although the study is quite relevant for the design of total ankle replacement prosthesis, is limited by considering only a single load and simulating only a balanced standing position.

Rodrigues [60] studied the stress patterns on the ankle joint for a normal ankle and for a prosthetic ankle. Three different prostheses were tested: the Agility^{TM}- for two different designs - and the S.T.A.R.^{TM}. This work included also a bone remodeling model, which predicts the optimal distribution of bone density after the implantation of the prostheses. The simulations were performed for 3 different states of the gait cycle - dorsiflexed, neutral and plantar flexed ankle - and the results showed that the stresses noted on the prostheses' polyethylene component surpassed the maximum allowed stress in the case of a dorsiflexed ankle. The results also showed that the internal stress distribution of the talus

changed drastically after the insertion of all the prostheses, with an increase of stresses in trabecular bone. This change of the stress patterns was suggested to explain the early loosening of the talar prosthetic component and influence the bone remodelling process [60].

Until now, the main goals of FE models have been to study stress and pressure patterns as well as bone remodelling processes in the ankle. Ligament stress and deformation have not been, however, studied as deeper as the cartilage stress and pressure. In 2012 Wei et al. [61] published a work in which the objective was to estimate not only ligament strains, but also to measure joint moments in the ankle after a grade I ATFL sprain. The model was composed of 5 bony segments including the tibia, fibula, talus, calcaneus and tarsal and metatarsal bones. All bones were considered rigid bodies, whereas the 20 ligaments modelled were formulated as linear elastic, tension only springs. An initial strain of 2% was implemented in all springs, inducing an *in situ* preloading of the ligaments. The input forces for the model were retrieved from a kinematic study where a male athete accidentally sprained his ankle while performing a cutting motion in a laboratorial environment. The ligamentous maximum strains, presented in Figure 2.10, were evaluated in 4 different movements - pure inversion, inversion plus PF, inversion plus internal rotation and a combination of inversion, internal rotation and PF - and denote that the ATFL has a high strain for the combination of inversion, PF and IR. These movements are known to take part in ankle lateral sprains and the values present in Figure 2.10 help to explain why the ATFL is the main injured ligament in that tye of ankle injury, followed by the CFL.

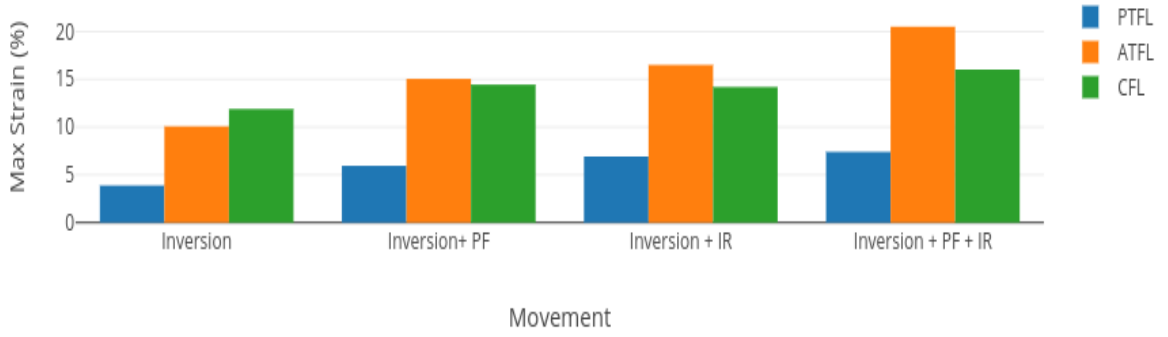

Figure 2.10: Maximum strains for the ATFL, CFL and PTFL, considering the movements of inversion, inversion plus PF, inversion plus internal rotation and a combination of inversion, internal rotation and PF. Adapted from Wei et al. [61].

Wang et al. [62] developed a 3D ankle model to evaluate 3 surgical techniques of the reconstruction of lateral ligaments: reconstruction of one-half of the peroneus longus tendon, reconstruction of one-half of the peroneus brevis tendon and allogeneic tendon reconstruction. The evaluation was done by resorting to the talar tilt and the anterior drawer tests. Figure 2.11 displays the FE model developed.

Comparing with the previous models, the main change introduced by this model concerns the mechanical properties of the ligaments, which were assumed to be nonlinear hyperelastic, with its constitutive relation following the neo-Hookean model [62]. The results for both the talar tilt and anterior drawer test can be seen in Tables A.1 and A.2, present in the Appendix section.

For the case of the anterior drawer test, the ATFL and CFL equivalent stresses in the case of allogeneic tendon reconstruction were very close to the stresses from the normal individuals' respective

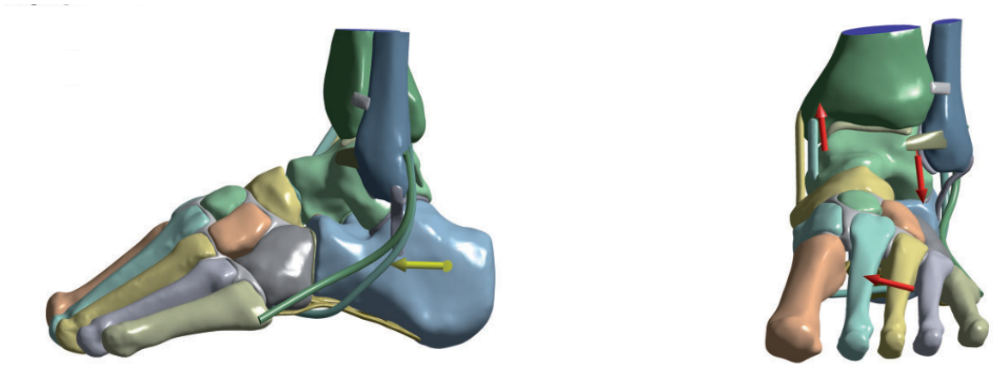

(a) (b)

Figure 2.11: (a) Lateral image of the ankle model used to simulate the anterior drawer test - displacement direction is in yellow (b) frontal image of the ankle model with the red arrows representing the forces applied in the talar tilt test. Adapted from Wang et al. [62].

ligaments, even closer than the results from the other two techniques. Considering the talar tilt technique, the results also showed that the allogeneic tendon reconstruction emerged as a better alternative for patients with torn LCL, comparing with the reconstruction of the peroneus longus and brevis tendons.

The work developed until now created the roots for further investigation in terms of not only ligamentous injuries, but also cartilaginous injuries. However the work done until now in the field of FE modelling of the ankle joint still does not answer to the questions related to ankle injury after joint rotation. This work aims to fill one of the gaps in ankle injury mechanisms, namely in the rotational instability, by evaluating the cartilaginous pressure patterns after LCL ligamentous injury.

2.5.1 Novel Aspects of the Work

Until now, the FE models existent were used to model the ankle in physiological conditions, or with small changes to that condition, simulating only particular injuries. Moreover, studies regarding ankle instability were not found in the literature, with this work being important to clarify the implications of ligamentar injury on the ankle cartilaginous pressure patterns, particularly of the rotational instability caused by the LCL injury. This ankle instability due to ligamentar injury, has proven to be a precursor of cartilaginous alterations, which can lead to OA over time [63].

Along with the cartilaginous pressure patterns, this work also pretends to confirm the importance of LCL on the IR since it only has been investigated in *in vivo* experiments. In fact, the quantification of strain on the ligaments in case of injury can help in the design of orthotic devices and in the customization of prevention, diagnosis and treatment strategies [64].

The work done by Guerra-Pinto et al. [5], described above, serves as premise for this thesis, with the findings from their work to be considered as a novel approach for the diagnosis of ankle LCL rupture - the pivot test. In fact, the IR angles used, the positioning of the axis of rotation and the boundary conditions applied were all based on the its work. The work developed in this thesis pretends to complement it numerically by evaluating the pressure patterns on the AJ cartilages, the ligamentous strains and the reaction moments of the ankle for the IR situations described in the work from Guerra et al..

Chapter 3

Methods

This chapter includes an explanation of the procedure involved in the development of the 3D ankle model, including the particular steps describing the generation of the bones (tibia, fibula, talus, calcaneus, navicular and cuboid), cartilages and ligaments. Then, the process of assembling all the parts is described, as well as the finite element (FE) analysis, including the material properties, the definition of interactions, load cases, boundary conditions and mesh generation.

3.1 Parts

The 3D modelling of the bones starts with a acquisition of a CT scan from the region of interest. The use of the CT images is very useful due to the fact that bone possesses a high contrast signal comparing with soft tissues [65]. In this case, a CT from a 23 year old male was used. Segmentation of the bones was performed in ITK-SNAP® (version 3.6.0, 2017) software, which is an open source software that focuses in providing semi-automatic segmentation of body structures using medical images. The input for this software is a set of CT slices which are prone to be reconstructed. The next step is to define a small region of interest, that contains only the bone which is going to be segmented, and to decide on the method of segmentation. The medical images comprise information, not only relative to the human body, but also undesired signals such as artifacts or blurred edges [66]. Due to this fact, a set of three techniques is used to perform bone segmentation: global thresholding, active contour method and manual segmentation.

Global thresholding consists in identifying and selecting the adequate intensities which identify a certain tissue - foreground - and annul the background. The values from the thresholded image go from -1 to 1 with the limits corresponding to the background and foreground respectively. Pixels that contain values near 0 indicate an edge between foreground and background [66].

The active contour method is an approach which consists in placing a group of closed surfaces - in this case spherical surfaces with variable radii - near the region of interest. These surfaces possess physical properties and deform, adapting to the image features, under external or internal mechanical forces [66]. These forces are calculated iteratively and, while internal forces contribute for smooth surface variations, external forces cause the adjustment of the model to the boundaries. An example of the iterative evolution of the active contour method and of the 3D evolution of the active contour method are pictured in Figure 3.1.

Due to the limitations of CT images, namely at the voxel size, and the small, but inherent, inaccuracy of the active contour method, a final manual segmentation was performed, more specifically in regions that have low bone density but are to be included in the final model. The final 3D model containing the tibia, fibula and the talus is presented in figure 3.2. After this first process, a surface mesh is generated

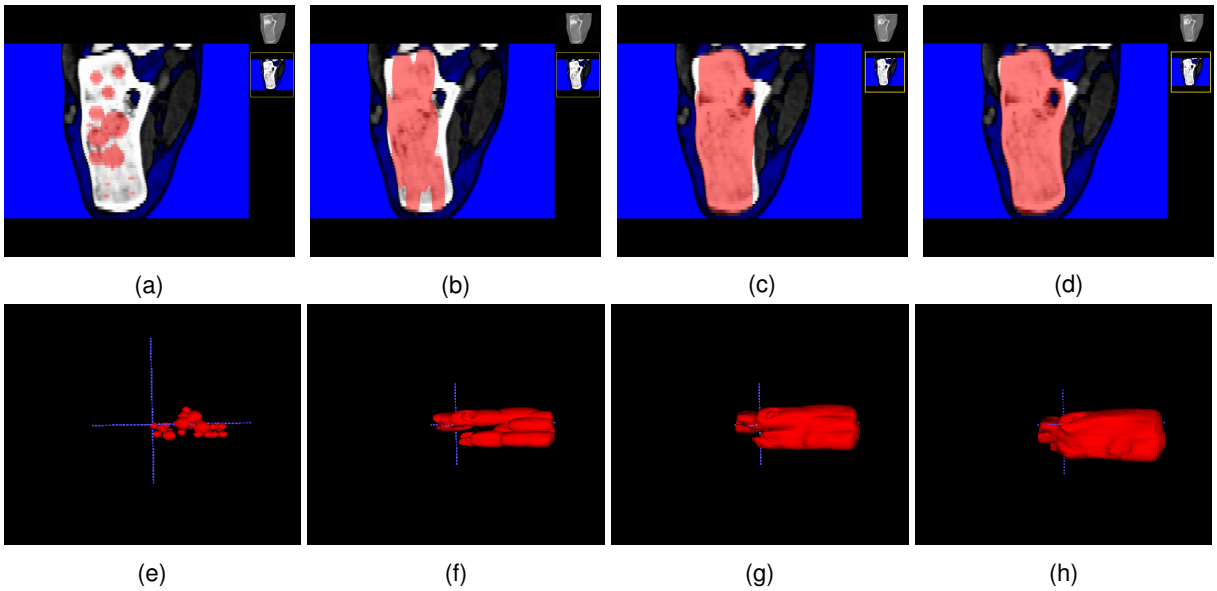

Figure 3.1: Axial view of the evolution of the active contour method of the calcaneus bone for (a) t=0, (b) t=50, (c) t=100, (d) t=150 and sagital view of the 3D evolution of the active contour method of the calcaneus bone for (e) t=0, (f) t=50, (g) t=100, (h) t=150.

by ITK-SNAP and imported to MeshLab [67].

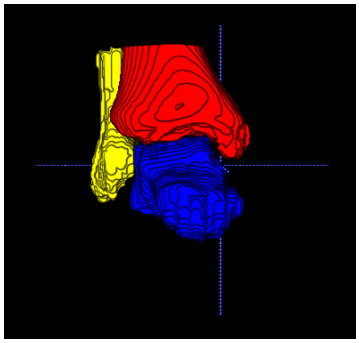

Figure 3.2: Final segmentation of the tibia, fibula and talus after active contour and manual segmentation methods.

The output from the segmentation presents both a stair-step shape surface, not corresponding to the real surface curvature, and an excess of nodes and faces that do not express relevant information. Due to these artifacts, the mesh must be adjusted using a smoothening technique. MeshLab [67] was the software selected for the quality improvement of the mesh. The smoothening technique consists in adjusting the nodal coordinates relatively to each other, keeping the mesh topology. Laplacian smoothening emerges as an effective and frequent filter used to amend the stair-step-like artifacts, improving the mesh surface. Figure 3.3 illustrates the result of applying the Laplacian filter to the talus.

The final step for the solid model generation includes importing the surface mesh into SolidWorks® (Student Edition, Academic Year 2016-2017). There, the ScanTo3D® toolbox was used to create the solid model of the foot bones and their native surface meshes. To improve computational efficiency, the proximal ends of both the tibia and fibula were cut using the same plane and, therefore, were not taken into account for the subsequent simulations.

In theory, the ankle cartilage can also be segmented through the same process as bone, but using a different image modality. MRI is the most used modality, because it allows for the direct visualization of the articular cartilage. Along with the CT scan used, also a MRI of the same ankle joint (AJ) was acquired. However, it did not have enough image quality so that the cartilages could be segmented from

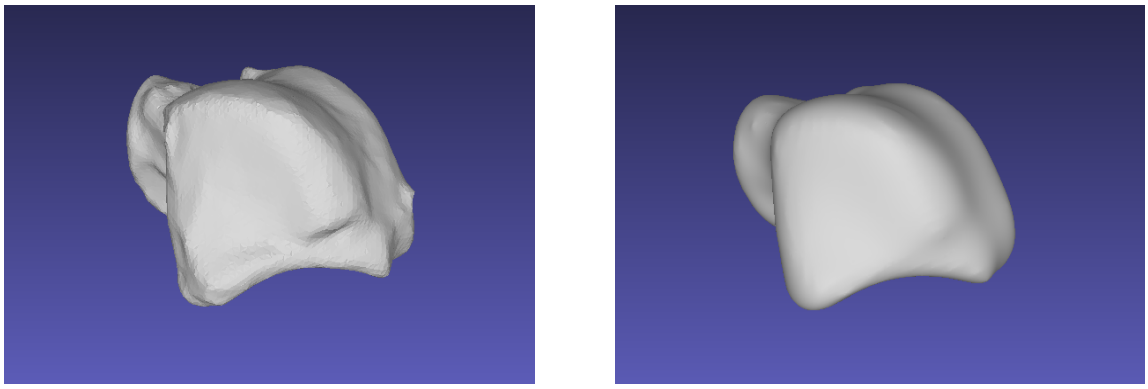

(a) (b)

Figure 3.3: (a) Imported talus model from ITK-SNAP and (b) talus model after the Laplacian filtering.

it. For that reason, the cartilages of the AJ were virtually simulated. For the tibial and fibular cartilage, a extrude of their surface mesh was made [68]. Extruding a surface is a process in which a 3D solid is created from an enclosed surface with a specific thickness. For the talar cartilage, since the surface is highly irregular - reason why the extrude of its surface was not a possible option - a different approach was taken. First, the original bone was scaled up 1.2 times the original size and then subtracted the normal-sized bone, creating a shell with the desired thickness [60]. Since there is no cartilage all over the bone, the next step was to define the areas with cartilage and remove the unwanted areas. The thicknesses of all three cartilages are of 1.5 mm for the talar cartilage, of 1 mm for the tibial cartilage and of 0.7 mm for the fibular cartilage, which are consistent with the *in-vivo* work done by Millington et al. [69]. Because the objective of this work is to evaluate the contribution of the lateral ligaments in the cartilage contact pressure, the interosseous membrane was not included in the model, since it is not expected to have a relevant impact on the results [60]. The final solid model imported into ABAQUS is shown in Figure 3.4.

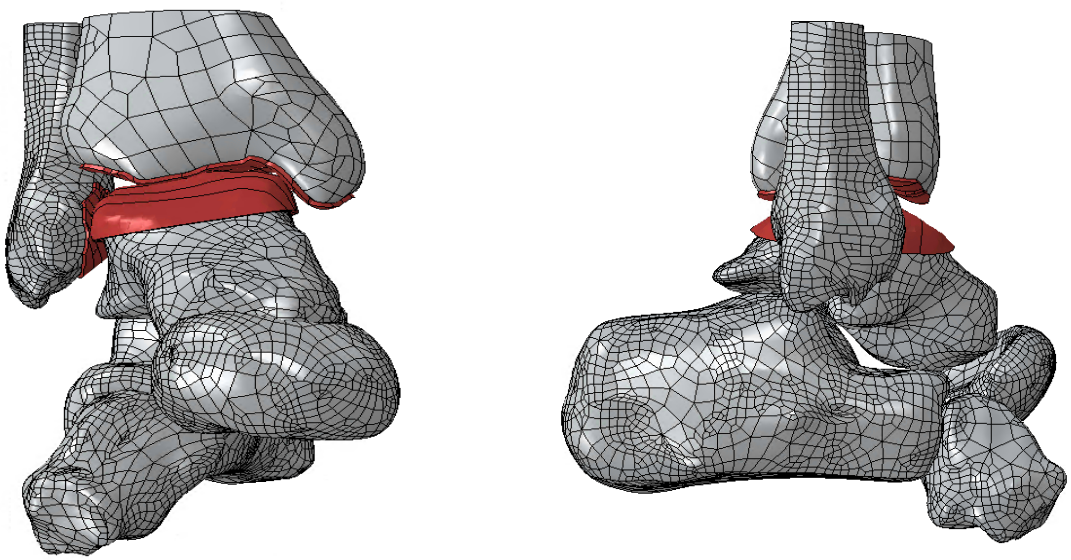

(a) (b)

Figure 3.4: Final model of the foot imported into ABAQUS®, with the bones in grey and the cartilages in red. (a) frontal view of the model and (b) lateral view of the model.

3.2 FE Modelling

3.2.1 Ligament Insertion

The full model was imported from SolidWorks® to ABAQUS® and the first step was to create and connect the ligaments. The choice of the nine ligaments used came from the study of Rasmussen et al. [70] about the stability of the ankle joint, the study from Corazza et al. [71] and the work from Guerra Pinto [5]. Three medial collateral ligaments (MCL) - PTTL, ATTL and TiNL -, three LCL - PTFL, ATFL and CFL - and three other ligaments - calcaneonavicular ligament (CNL), cuboideonavicular ligament (CuNL) and the calcaneocuboid ligament (CaCL) - were modelled. Figure 3.5 depicts an example of all the ligaments from the FE model and their representation in the literature.

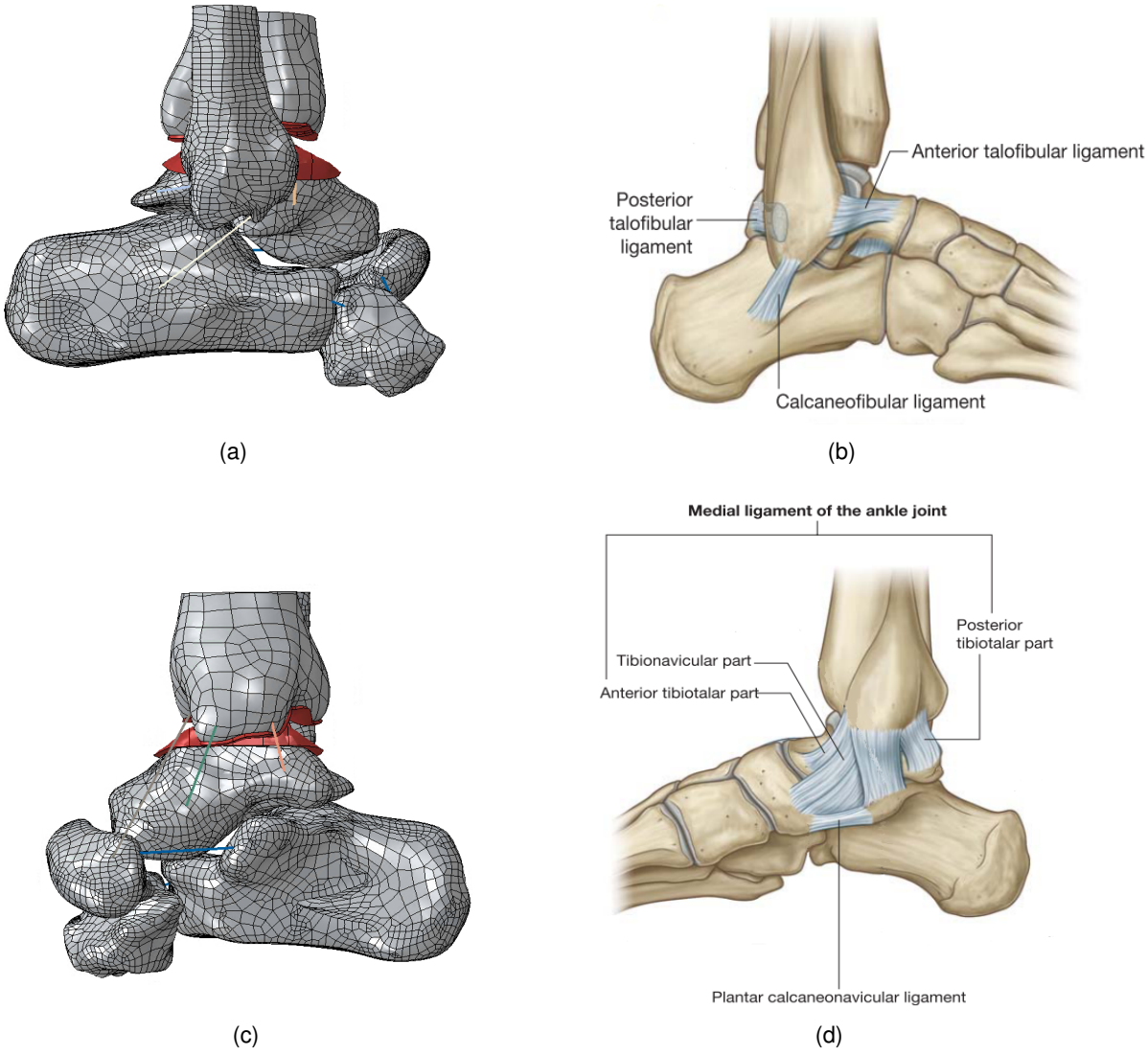

(a) (b)

(c) (d)

Figure 3.5: (a) FE model of the LCL and other tarsal ligaments. From left to right: PTFL in light blue, CFL in white, ATFL in pink, CaCL in blue and CuNL also in blue; (b) Representation of the LCL. Adapted from Drake et al [17]; (c) FE model of the MCL. From left to right: TiNL in grey, STTL in green, CNL in blue and PTTL in orange; (d) Representation of the MCL. Adapted from Drake et al [17].

All ankle ligaments have different attachment surfaces. The definition of these areas was carefully done so that there is a close resemblance between the computational model and the anatomical model. However, because there are no 3-D coordinates of the attachment surfaces for the ligaments, the inser-

tion areas were created based on anatomical descriptions and medical images [23]. Then, reference points (RP) were created and coupled to the insertion area using a coupling constraint of ABAQUS®. This option ensures that the ligament is attached to the insertion surface and that the forces are uniformly distributed on the surface, mimicking what happens in the human body, while avoiding stress concentration points. All the ligaments modelled are illustrated in Figure 3.5.

The ligaments were modelled using tension only truss elements. This was attained using the "no compression" option defined by ABAQUS®, in which the parts have their elastic behaviour modified and do not generate tension under compression.

To represent in situ levels, a prestretch of 2% was applied to every ligament according to the work of Liacouras et al. [72].

3.2.2 Material Properties

The non-linear properties of the biological is difficult to reproduce in computational models. Therefore, several approximations have to be considered for the mechanical properties of bone, cartilage and ligaments. In this work, bone is considered a linearly elastic, homogeneous - no difference between cortical and trabecular bone - and isotropic material, so that it is not directionally dependent [73]. In fact, this arises as one of the limitations of this work, since the stress and deformation of bone depend closely on its structure, and on the consequent mechanical properties [73]. Bone was assigned an Young's modulus of 7.3 GPa and a Poisson's ratio of 0.3 according to Cheung et al. and Gefen et al. [55, 74].

Cartilage has a viscoelastic behaviour [54], but was modelled here using a linear elastic and isotropic law with a Young's modulus and Poisson's ratio of 10 MPa and 0.4 - due to its almost incompressible nature.

The ligaments were modelled also as linear elastic and isotropic and were considered to have different Young's moduli and cross sectional areas, but the same Poisson's ratio. The values considered were taken from the works of Corazza et al., Liacouras et al., Siegler et al. and Cheung et al. [71, 74, 72, 75]. No data were found for the CNL, the CuNL and the CaCL. However, the value of 260 MPa was used accordingly to the work done by Ozen et al.[59], and the cross-sectional area was calculated using the relationship between a spring's constant of a rod and the Young's modulus of that same rod:

$$k = E\frac{A}{L} \tag{3.1}$$

where k is the spring's constant - assumed to be 70 N/mm according to the work of Liacouras et al. [72] -, E is the Young's modulus, A is the cross-sectional area and L is the length of the ligament. In terms of Poisson's ratio, all ligaments were assumed to be incompressible, assuming ν =0.46. The mechanical properties for all ligaments are presented in Table 3.1

3.2.3 Model Interactions

The interactions between bone and cartilage were considered rigidely bonded using a tie constraint. Cartilage on cartilage interactions were simulated using a surface-to-surface contact formulation. Because the interaction between articular surfaces can be considered almost frictionless [59], a coefficient of friction of 0.01 was considered [76].

Table 3.1: Mechanical properties for all the ligaments considered in this work, as well as the cross-sectional area for each ligament. The material properties were taken from Corazza et al., Liacouras et al., Siegler et al. and Cheung et al. [71, 74, 72, 75].

Ligament	Young's Modulus, E (MPa)	Poisson's Ratio, ν	Cross-sectional area (mm^2)
ATFL	225.5	0.46	12.9
PTFL	216.5	0.46	21.9
CFL	512	0.46	9.7
TiNL	320.7	0.46	7.1
ATTL	184.5	0.46	13.5
PTTL	99.54	0.46	45.2
CNL	260	0.46	0.7
CuNL	260	0.46	105
CaCL	260	0.46	98.67

3.2.4 Loads

The main focus of this work is the internal rotation (IR) of the talocrural (TC) joint. Nevertheless, the presence of a compressive force to induce the contact of the cartilages is required. There is no bibliography for a minimum compressive force to generate the wanted cartilage contact, so a sensitivity analysis was performed and the maximum pressure felt by the talar cartilage was measured for different compressive force magnitudes - namely 5, 8, 10, 15, 20 and 40 N.

The results were the expected, as the maximum pressure grew linearly with the load and, as this work follows the directions of the study made by Guerra-Pinto et al. [5], a minimal compressive load was chosen - of 10 N - to initiate, as stated earlier, the contact between cartilages.

3.2.5 Boundary Conditions

Before assigning all the boundary conditions, the axis about which the rotation will be performed, must be defined. This was attained by creating an axis that resembled the longitudinal rod which served as pivot in the work of Guerra-Pinto et al.[5]. This axis went through the plantar area of the foot, 0.5cm away from the medial shoulder of the talus and through the distal aspect of the tibia, in line with its sagittal and coronal axis. From hereafter, this axis will be refered as MA.

Regarding the boundary conditions of the model, the tibia and the fibula were fixed in their proximal surface, meaning that the degrees-of-freedom of the surface nodes are completely fixed. For the sake of computational simplicity, the tarsal bones - talus, calcaneus, navicular and cuboid - were defined as rigid bodies using a rigid body constraint. A rigid body consists on a group of nodes, elements and surfaces which have their motion controlled by the motion of a single reference node. Thus, not only the relative positions of the nodes and elements that are comprised by the constraint remain constant during the simulation - not allowing for deformations - but also the motion of the whole group of bones can be made by simply applying boundary conditions at the single reference node. The reference point was chosen as the point at which the MA goes through the distal surface of the talus.

To constraint the movement of the rigid bodies, the reference point controlling the rigid bodies was constrained to allow only their translation along the MA direction and their rotation about the same axis.

As described earlier, there are 3 cases of rotation for 3 different ligamentous configurations. The loading conditions were applied in two steps. In the first step, only the compressive load of 10 N was considered, and the rigid body reference point could only move in the direction of the MA. The second step included also the compressive force of 10N, but an IR around the MA was applied, depending on the ligamentous configuration - 3.67°for the intact ankle, 9.6°after the anterior talofibular ligament (ATFL) section and 13.43°after ATFL and calcaneofibular ligament (CFL) section. The values for the rotation

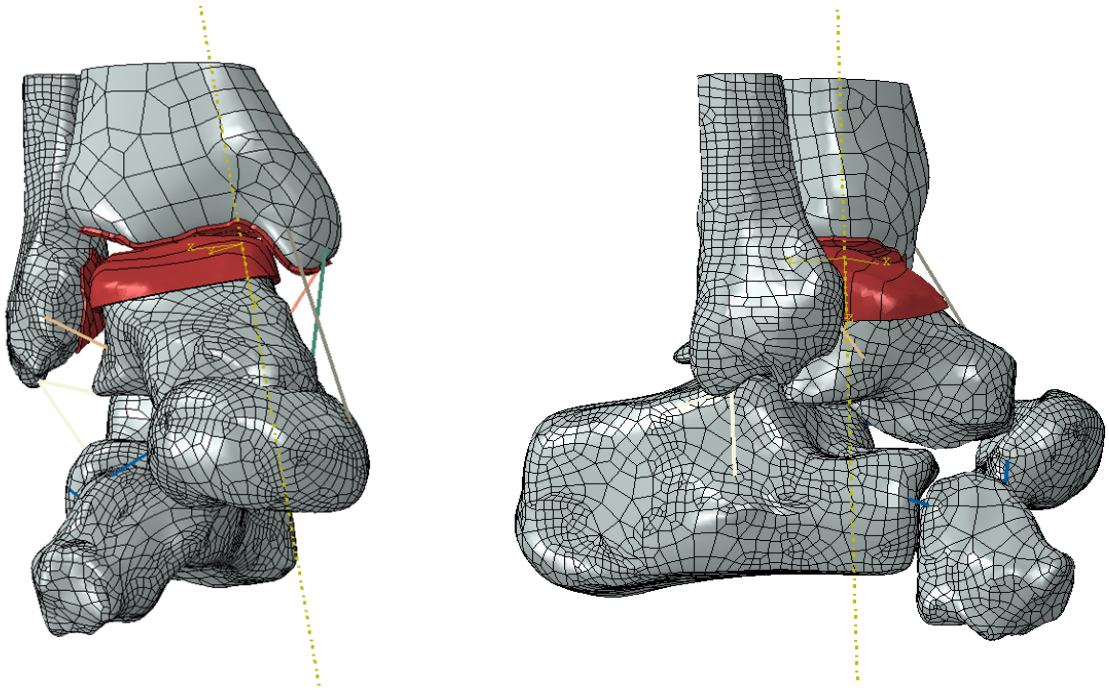

(a) (b)

Figure 3.6: (a) frontal image and (b) lateral image of FE model of the ankle with the MA and the coordinate system highlighted in yellow.

were taken from the work of Guerra et al. [5]. Table 3.2 summarizes the forces and rotations applied for each step, taking into account that ABAQUS® requests the angles to be given in radians and not in degrees.

Table 3.2: Loads and rotations applied for each step in this model. The loads and rotations are negative due to the orientation of the local coordinate system.

	Step 1 Compression	Step 2 Rotation	
	Loads (N)	Loads (N)	Rotation (°)
Intact ankle	-10	-10	-3.67
After ATFL cut	-10	-10	-9.6
After ATFL and CFL cut	-10	-10	-13.43

3.2.6 Mesh Generation

After defining all the constraints and loads for the model, the last step before the simulations is the mesh generation. ABAQUS® gives two 3-Dimensional options for meshing: tetrahedral and hexahedral meshing. While tethahedral elements can be more easily automated and has been the choice for most of foot models and biomechanical research, hexahedral elements have a higher performance in terms of convergence rate and accuracy of the solution [77]. In this work, bones were described by linear tetrahedral (C3D4) elements, due to their complex geometry, cartilages were modelled by linear hexahedral (C3D8) elements, since they allow for a better contact according to Tadepalli et al. [77], and ligaments were defined by linear trusses. To ensure the finite element meshes were computationally efficient but accurate enough, and proceed to the mesh choice, a convergence study was done using a compressive

force of 650 N (equal to the weight of the subject). The mesh of the cartilages were refined from 1.5mm to 0.3mm, while the value of the maximum pressure on the talar cartilage was measured. The values for the maximum pressure depending on the mesh size can be seen in Figure 3.7

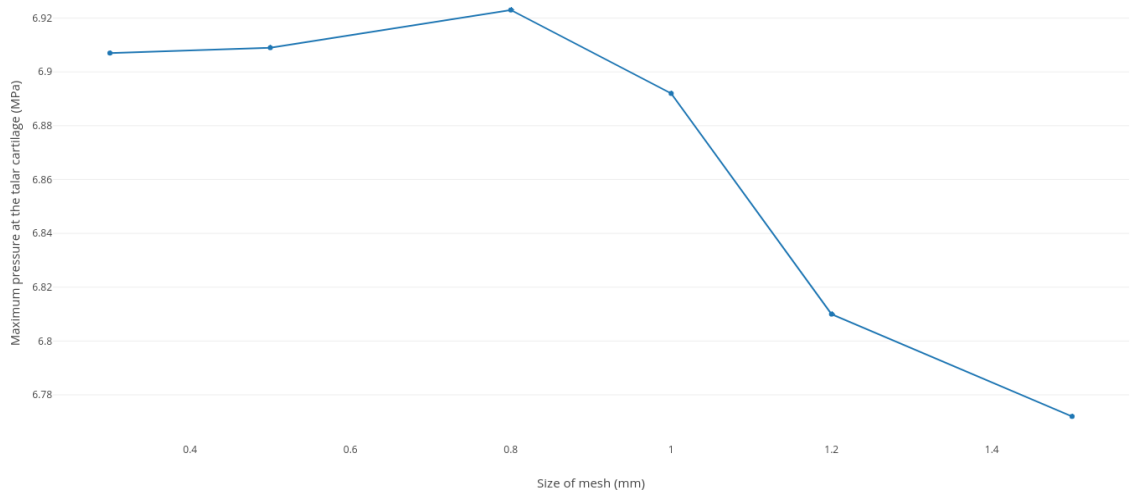

Figure 3.7: Values for the maximum pressure felt on the talar cartilage (MPa) depending on the mesh size (mm) for a compressive force of 650 N.

The differences in the pressure at the talar cartilage were not significant for the mesh sizes evaluated. For example, from the size of 1 to 1.2 the difference was of 1.2%, being the biggest difference calculated. However, by looking at Figure 3.7 it is possible to observe that the maximum pressure stabilizes after the mesh with 0.8 mm, thus, and for the sake of both computational efficiency and quality of the results, a size of 0.5 mm was chosen for the cartilages.

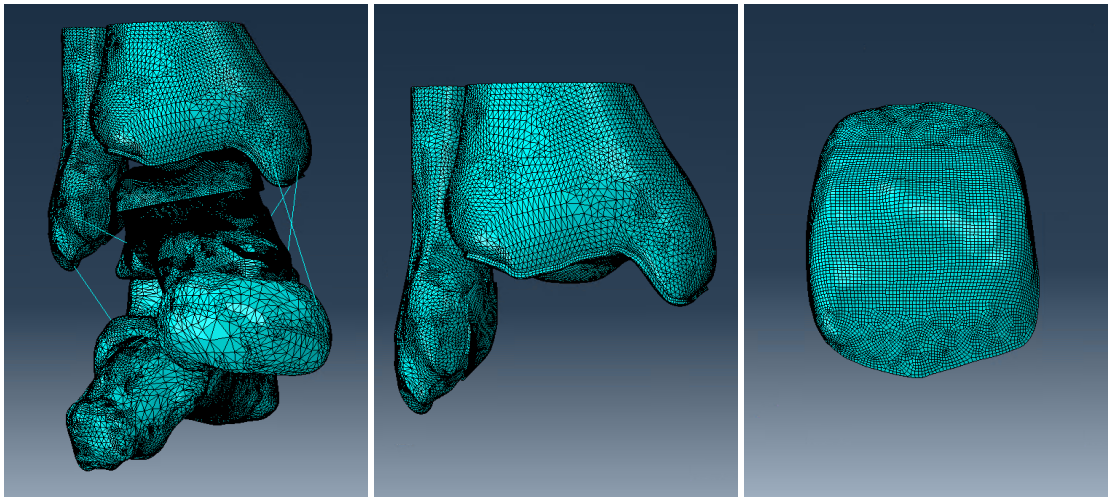

(a) (b) (c)

Figure 3.8: (a) Ankle meshed FE model; (b) tetrahedral FE mesh of the tibia and fibula and hexahedral FE mesh of the tibial and fibular cartilage; (c) superior view of the hexahedral FE mesh of the talar cartilage.

As for bone, no convergence analysis was done, since no important informations are going to be taken from it. However, for the tibia and fibula a refined mesh should also be implemented since it could influence the results on the cartilage [77]. Due to this, a mesh size of 1 mm was chosen, taking in

accordance the study done by Tadepali et al [77].

The ligaments were meshed using a linear truss mesh with the size equal to the size of the ligament.

An example for the bony, cartilaginous and ligamentous FE mesh can be seen in Figure 3.8

3.2.7 Results Presentation

In this work, the contact pressure, the ligamentous strains and the reaction moments were calculated and analyzed.

Contact pressure was extracted for each cartilage - talar, tibial and fibular - and only the maximum pressures are highlighted.

Ligamentous strains were calculated by evaluating the initial size of the ligaments before and after rotation and computing the Cauchy strain formula:

$$\varepsilon = \frac{\Delta L}{L} = \frac{l - L}{L}, \tag{3.2}$$

where ε represents the strain of the ligament, L is the initial size of the ligament and l is the final size of the ligament.

Reaction moments, which are the reactions induced by the ligaments and the cartilaginous contact after the ankle rotation, were extracted for the entire model and only the reaction moment around the MA was considered. For the simulation of the reaction moments, a slightly different approach was taken, in which the 3 rotations considered for this work were applied to all 3 ligamentous configurations, with a total of 9 reaction moments calculated.

Chapter 4

Results and Discussion

In this chapter, a validation for the model is presented, followed by the results for pressure distribution, ligament stress and strain and resultant moments. The results are then compared with existing clinical and experimental results obtained by other authors.

4.1 Model Validation

The model validation was done using the work done by Kimizuka et al [1], in which the load-bearing patterns of the ankle joint, namely contact areas and pressure distribution of 7 healthy human TC joints, were measured. The measurements were made by applying, on the plantar aspect of the foot, a set of 3 compressive loads with 500 N, 1000 N and 1500 N. The contact pressure was measured *in vivo* using a thin pressure sensor made of polyester. The *in vivo* experiment was recreated using the FE model developed and the 500 N, 1000 N and 1500 N compressive forces were applied, with the maximum pressures felt by the talar cartilage being measured afterwards.

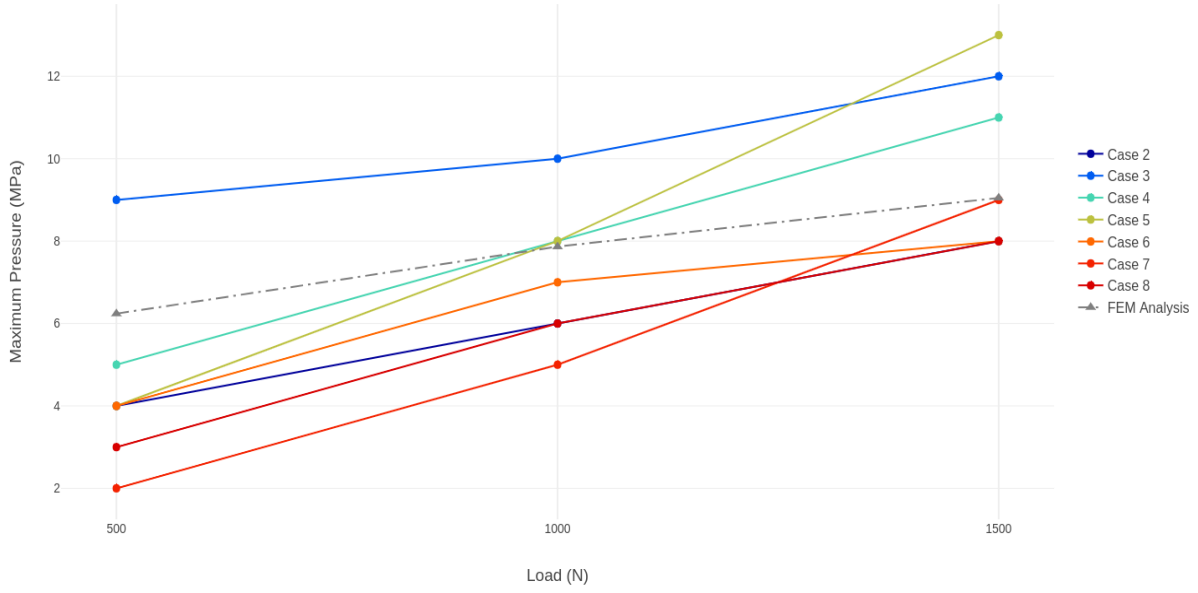

Figure 4.1: Plot of the 7 different cases' maximum pressures measured in the talar cartilage from the study of Kimizuka et al [1] in different colors and the FE method values in grey.

The maximum contact pressures measured by Kimizuka et al. [1] and those estimated here are depicted in Figure 4.1. For a more quantitative analysis, the results are further detailed in the Appendix A.3. As seen in figure 4.1, the grey line denotes the results obtained by the FE method while the other lines correspond to the 7 different cases of the work of Kimizuka et al. [1]. The computational results are within the range of the experimental results, implying that the FE model is well built quantitatively in terms of compressive response.

Figure 4.2 compares the patterns of pressure distribution for a load of 1500 N. Although the pressure on the FE model is not as lateral as the one on the *in vivo* cartilage, a similar pattern is observed in both contact pressures. The spatial difference can be explained by the orientation of the ankle before the compressive force being applied. In the work done by Kimizuka et al [1], the compressive force was applied in a neutral positioned ankle along the longitudinal axis, while in the FE model, the ankle might not have been in a completely neutral position. The circles of pressure are also somewhat different from the FE model to the model from Kimizuka et al. Both the figures for compressive forces of 500 N and 1000 N can be found in the Appendix A.

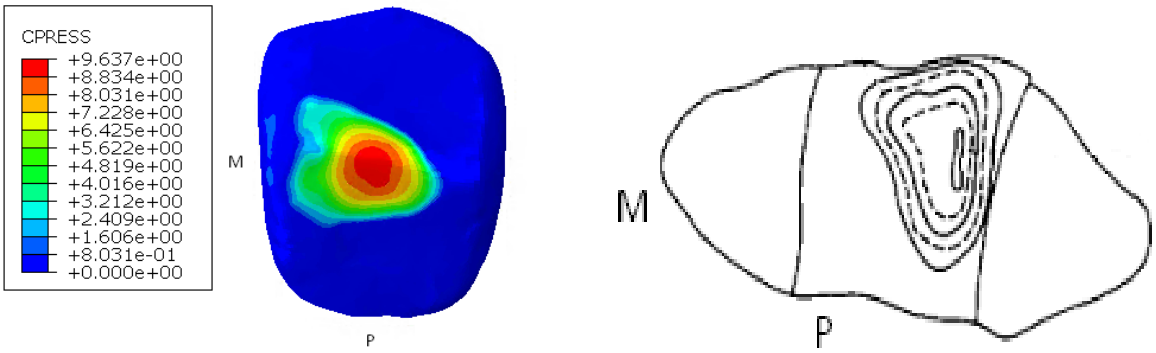

(a) (b)

Figure 4.2: (a) FE model of the talar cartilage with the contact pressure values for the 1500 N compressive load. The maximum contact pressure is in red and corresponds to 9.637 MPa and the medial and posterior orientations are marked with a ”M” and ”P” respectively. (b) *In vivo* pattern of pressure distribution taken from the work done by Kimizuka et al [1].

4.2 Cartilage Pressure

4.2.1 Results

The computed contact pressures for the talar, tibial and fibular cartilages are displayed in figures 4.3, 4.4 and 4.5. Three rotational conditions are considered in this analysis. At first, for an intact ankle, a rotation of 3.67°is applied, and the results are presented in figure 4.3. The fibular cartilage is not presented since it had no contact pressure.

The second case is done after the anterior talofibular ligament (ATFL) cut and applying a rotation of 9.6°. The results for this case can be observed in figure 4.4.

Lastly the contact stresses for the same three cartilages but with the cut of both the ATFL and calcaneofibular ligament (CFL) and an IR of 13.43°are presented in figure 4.5

The results show not only a change on the contact pressure patterns with the different angles of IR, but also a growth of the maximum pressure noted in every cartilage. Comparing qualitatively the contact areas on the talar cartilage, a continuous increase is observed fro 3.67°to 13.43°of IR. Anteromedial and posterolateral contact on the talar cartilage started to occur only for the IR rotations considered

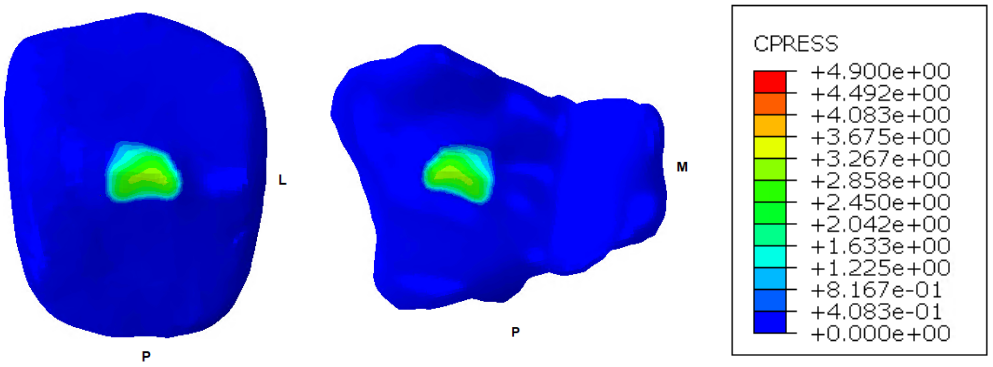

(a) (b) (c)

Figure 4.3: Contact pressure (MPa) in the (a) superior surface of the talar cartilage and in the (b) inferior surface of the tibial cartilage for an internal rotation (IR) of 3.67°with (d) being the scale in MPa. M, L and P stand for medial, lateral and posterior orientations respectively.

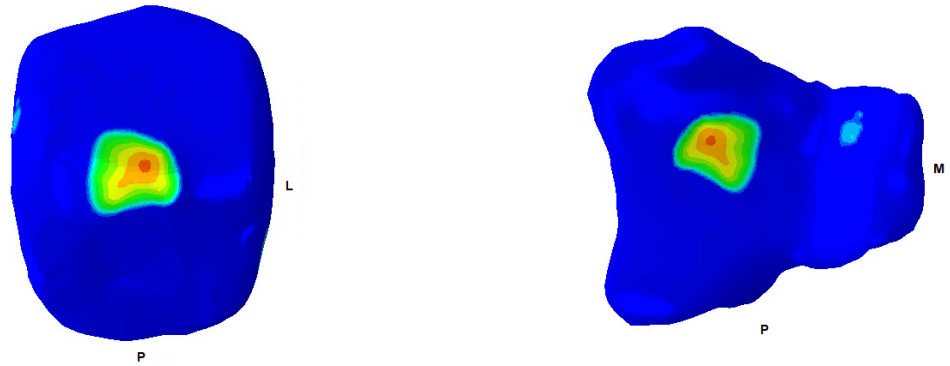

(a) (b) (c) (d)

Figure 4.4: Contact pressure (MPa) in the (a) superior surface of the talar cartilage in the (b) inferior surface of the tibial cartilage and in the (c) medial surface of the fibular cartilage, for an IR of 9.6°with (d) being the scale in MPa. M, L, P and S stand for medial, lateral, posterior and superior orientations respectively.

larger than 3.67°. Regarding the contact pressures, a quantitative analysis was done by evaluating the maximum pressures for the three cases of rotation, which are presented in Table 4.1. The maximum pressures are in the range of 2.23-4.77 MPa, with the fibular cartilage having no pressure for an IR of 3.67°. By increasing the angle of IR, the maximum pressure also increases.

In conclusion, for the smaller IR angle, both the contact areas and maximum pressure values are smaller when compared with the values of 9.6°and 13.43°. There is also an occurrence of pressure ”hot

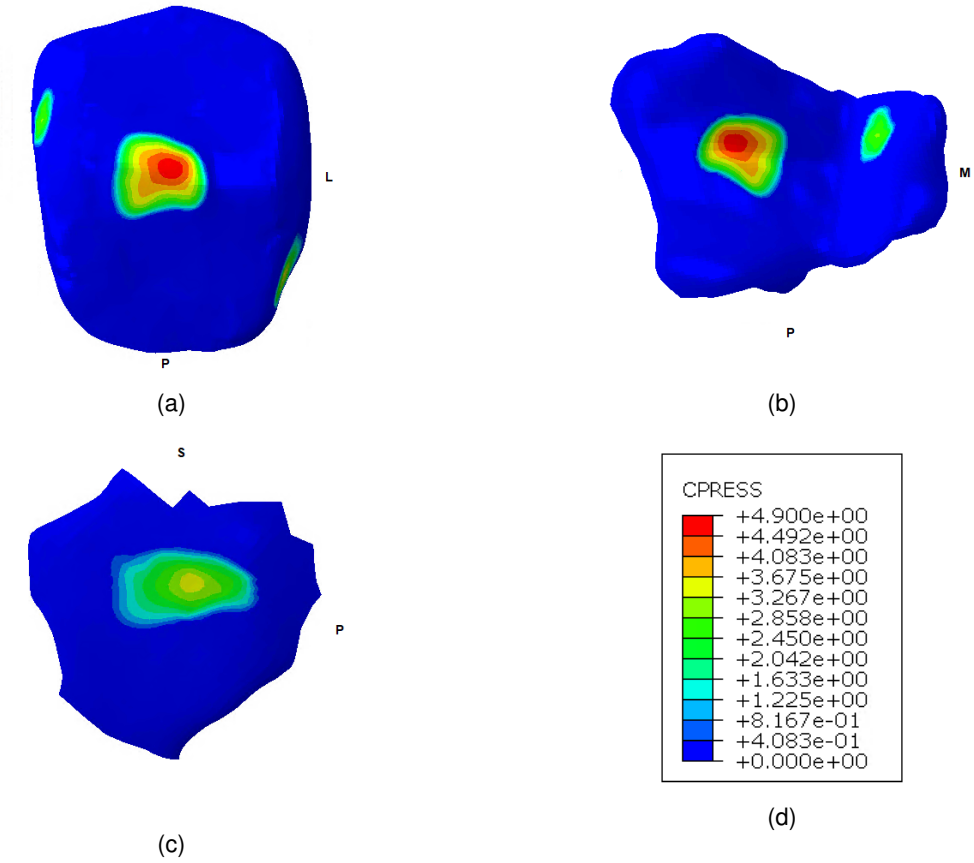

Figure 4.5: Contact pressure (MPa) in the (a) superior surface of the talar cartilage in the (b) inferior surface of the tibial cartilage and in the (c) medial surface of the fibular cartilage, for an IR of 13.43°with (d) being the scale in MPa. M, L, P and S stand for medial, lateral, posterior and superior orientations respectively.

Table 4.1: Values for the maximum pressure (MPA) on the fibular, tibial and talar cartilages for IRs of 3.67°, 9.6°and 13.43°.

	3.67°	**9.6°**	**13.43°**
Fibular cartilage	-	2.23	3.63
Tibial cartilage	3.09	4.15	4.75
Talar cartilage	3.11	4.15	4.77

spots" in the anteromedial and posterolateral areas of the talar cartilage, coincident with pressure spots on the medial side of the tibial cartilage and on the fibular cartilage respectively.

4.2.2 Discussion

When it comes to biological movements such as the gait, the analysis of the magnitude and distribution of contact pressures in the ankle joint as a function of the loading conditions and ankle position - plantarflexion (PF), dorsiflexion (DF) and neutral position - is already well described by numerous authors [1, 60, 78, 79]. After ligamentous injury, and a consequent state of ankle instability, the cartilage contact areas are still a less developed subject, due to the high randomness of movements for a 3D instability. However, by constraining the instability into just one plane - in this case the horizontal plane - it is possible to get a glimpse of the repercussions of the rotational instability in the ankle cartilages.

Taga et al. [10] examined 31 ankles with lateral ligament injury, where 9 patients had fresh injuries and 22 had chronic injuries, and the incidence of chondral lesions was very high - 89% for the fresh injured ankles and 95% for the chronic injured ankles. Most of the lesions observed were in the medial half of the ankle joint, especially on the anteromedial facet of the tibial cartilage, having higher lesion grades than lesions on the lateral side. One curious observation was that the extent of ligamentous injury had no effect on chondral lesions, meaning that, for example, an isolated ATFL injury was no better than a combined ATFL and CFL injury.

Hirose et al. [80] tried to confirm the association between lateral ligament injury and associated cartilage degeneration in the TC joint. After analyzing more than 100 cadavers and 128 ankles, they found that association to be valid. After separating ankles with lateral collateral ligament (LCL) injury and healthy ankles, they observed that degenerative changes were found more frequently in the first group than in the second one - 78.8% and 49.5% respectively. Also, the talar side was more affected than the tibial side, with the medial side of the dome having a higher incidence on the medial half of the dome - about 63.6% of the injured ankles - but also a representative incidence on the lateral malleolar facet - 42.4% of the injured ankles. Also, mirror-image lesions were found with higher incidence in injured ankles, with the medial facets of the tibia and talus being the most affected with 57% of the total mirror-image lesions.

Bischof et al. [81] also studied the contact strain maps in the TC joint, using 3D MRI models and biplanar fluoroscopy, and found that for a LCL injured ankle, the peak strains in the talar cartilage not only increase but also shift anteromedially, most likely due to not only a combined anterior translation and IR of the talus, but also due to the curved articular surface of the medial malleolus. Qualitatively, the strain patterns analyzed by Bischof et al. have the same shift as the pressure patterns observed in the FE.

By observing both the tibial and talar pressure patterns in Figures 4.3, 4.4 and 4.5, it is clear that for an healthy ankle, there are no pressure points in the medial facet of the tibial cartilage, as opposed to the pathological ankles. Clinical studies have shown that normal physiological loading does not harm the cartilage, since it responds in a very site-specific way to loads [19]. This can be explained due to a variation of the tensile modulus of an healthy human cartilage, depending on the location over the joint surface, meaning that high weight bearing regions have a higher tensile modulus and vice-versa [18]. Hence, cartilaginous areas that are not usually solicited by loads, will suffer lesions when abrupt, non-biological stresses are applied, such as the ones seen in the FE model. This falls in line with the hypothesis that, for pathological values of IR, pathological areas of pressure start to appear in the TC joint. Despite being more common the appearance of medial degenerative areas in the ankle cartilage, the presence of lateral injuries was also described by Hirose et al. and Bischof et al. [80, 81], validating the lateral pressure felt by the posterolateral areas of the talar cartilage and by the fibular cartilage. The lesion of the lateral ligaments and consequent ankle rotational instability induces a laxity state on the AJ, raising the probability of cartilaginous injury caused by the appearance of the pathological pressure patterns mentioned earlier.

To the author's knowledge, there are no ankle maximum contact pressure values documented. However, Brand documented in 2005 the peak stresses for the ankle cartilage [82] and, although the main goal of this work is to evaluate the contact pressure, the stresses felt by the ankle cartilage are also important to understand its degenerative process. In fact, Brand suggested that, in the same way as other tissues, cartilage also ignored the majority of the experienced mechanical signs and responded only to selected features, meaning that many submaximal loadings could have a higher deterioration rate than fewer maximal loadings. Table 4.2 shows the maximum von Mises stresses for the FE model and the peak stresses documented by Brand. The values denote that the FE model's peak stresses do not surpass the ones described in the literature - also due to a smaller load applied in the FE model.

Brand also hypothesized that, as cartilage responds differently depending on the area under stress, few submaximal cyclical loads could have degenerative effects if applied in more injury prone areas, such as the inner facet of the tibial malleolus - which is one of the most common areas of lesion in the AJ cartilage as described above - [82].

Table 4.2: Peak stresses for the talar cartilage of the FE model for IRs of 3.67°, 9.6°and 13.43°and the peak stresses of the ankle joint taken from the work of Wagner et al., Steffensmeier et al., and Calhoun et al. and gathered by Brand.

	Peak stresses (MPa)
FE model for 3.67°	2.139
FE model for 9.6°	2.808
FE model for 13.43°	3.692
Wagner et al. [83]	>6
Steffensmeier et al. [84]	8.9
Calhoun et al. [85]	3-8

To sum up, constraining the model to an axial rotational instability allows for a better understanding of the importance of the lateral ligaments on the contact pressure in the cartilage of the AJ, with the results obtained being consistent with previous medical studies of ankle instability.

4.3 Ligamentous Strains

4.3.1 Results

To understand the ligamentar strain and consequent importance in the control of the IR, the strains of the ligaments present in this model were evaluated and compared with strains reported in the literature.

Table 4.3 contains the relevant strains retrieved from the FE model depending on the degree of IR.

Table 4.3: Strains calculated for 5 ligaments - ATTL, PTTL, PTFL, CFL and ATFL - for the 3 degrees of rotation used in this work. Negative strains represent a shortening of the ligament whereas positive ones represent a stretching. The ATFL has been excluded from the 9.6% and 13.43% rotations and the CFL from the 13.43%, having no strains for that reason.

		Degrees of rotation		
		3.67°	**9.6°**	**13.43°**
Ligaments	**ATTL**	-3%	-7.2%	-9.2%
	PTTL	3.10%	8.7%	12.9%
	PTFL	-8.15%	-21.6%	-29.7%
	CFL	-2.8%	-4.5%	-
	ATFL	4.7%	-	-

According to Table 4.3, only the PTTL and the ATFL were stretched in the IR while all the other ligaments were shortened. In fact, the PTFL shortened 29.7%, being the ligament with the highest shortening, while the PTTL was the one with the highest stretching, with almost 13%, quadrupling the initial stretching value for 3.10%. The data for the ligaments not included in Table 4.2 are not presented because their strains were zero - these ligaments were connecting two bones covered by the rigid body constraint.

4.3.2 Discussion

The results obtained suggest that only the posterior tibiotalar ligament (PTTL) and the ATFL work against the movement of IR. In fact, there are multiple factors that can influence the stretching or shortening of ligaments on the IR. One of them is described by both Rasmussen [70] and Colville et al. [64]

which is the ankle position before IR. In this work, Rasmussen claimed that the ATFL seemed to be the essential structure in restricting the IR, founding ruptures of this ligament whenever a forced IR was applied. The CFL, although being initially thought to be also a major antagonist of IR, is described by Rasmussen to not have a big influence on this movement when the ankle is in a neutral position. However, for an adducted - or inverted - ankle, the CFL is highly recruited, with ruptures of this ligament being found for a forced IR, and the same importance for a dorsiflexed ankle - without IR. The PTFL is also thought of limiting the IR, but Rasmussen found that its influence was circumscribed to an IR of an adducted ankle, having no major influence nor straining in a neutral ankle IR. This findings are in line with the computed strains obtained from the FE model. One of the main questions posed by Rasmussen was if the PTTL had any influence in forced IR. In fact, it was reported by Dehne [86] that the PTTL was stretched at the same time as the ATFL in forced IR, implying that it would possibly prevent that movement, thus being important in the control of rotatory instability.

Colville et al. [64] measured the LCL strains for the IR of the ankle for a range of flexion of the ankle - from 20°of PF to a neutral position and then to 20°of DF - and found that both the CFL and the PTFL have little to no strain in a neutral ankle IR, whereas the ATFL had almost 10% of strain. The variations from the medical findings to the FE model results could be explained due to the ligament position on the model. For example, in the FE model, the CFL shortens, while in the *in vivo* experiments it has a minimal stretching, despite having low importance in the IR as stated above. The modelling of ligaments with a single truss instead of with multiple trusses representing the multiple fibers that compose them [17], along with a possible high sensitivity to the orientation of modelling, as explained above, represent major limitations of this work. Also, the axis of rotation could be inducing some degree of abduction - instead of a pure rotation - which, as also documented by Rasmussen and Colville et al. [70, 64], relieves some tension from the CFL and could be the cause of the ligament being shortened instead of stretched.

The extracted strains from the FE model are considered to be in line with the medical *in vivo* descriptions of ligament activation for a neutral internal rotated ankle. The ligament position in the FE model should, nevertheless, be better assessed with a sensitivity analysis.

4.4 Reaction Moments

4.4.1 Results

The values for the reaction moments on the model can be seen in table 4.4 and in figure 4.6. For this moments, IRs of 3.64°, 9.6°and 13.43°were applied for the models with intact ligaments, with ATFL cut and ATFL and CFL cut. The values presented were normalized by the reaction moment of the foot with intact ligaments and an IR of 3.64°.

Table 4.4: Values for the reaction moments (N m) taken from the FE model for the 3 rotation angles and for 3 different ligamentous configurations. Inside brackets are the normalized values by the reaction moment of the foot with intact ligaments and IR angle of 3.64°

Rotation Angle (º)	Intact ligaments	ATFL cut	ATFL and CFL cut
3.67	1.37(1)	1.27(0.93)	1.27(0.93)
9.60	4.99(3.64)	3.55(2.58)	3.55(2.58)
13.43	8.93(6.51)	5.94(4.32)	5.94(4.32)

The reaction moment increases with the rotation angle for the same ligamentous configuration and decreases with the cut of the ATFL for the same rotation angle. In fact, the value for the reaction moment for the model with intact ligaments increases almost 3.5 times from 3.67°to 9.6°and 1.8 times from 9.6°to

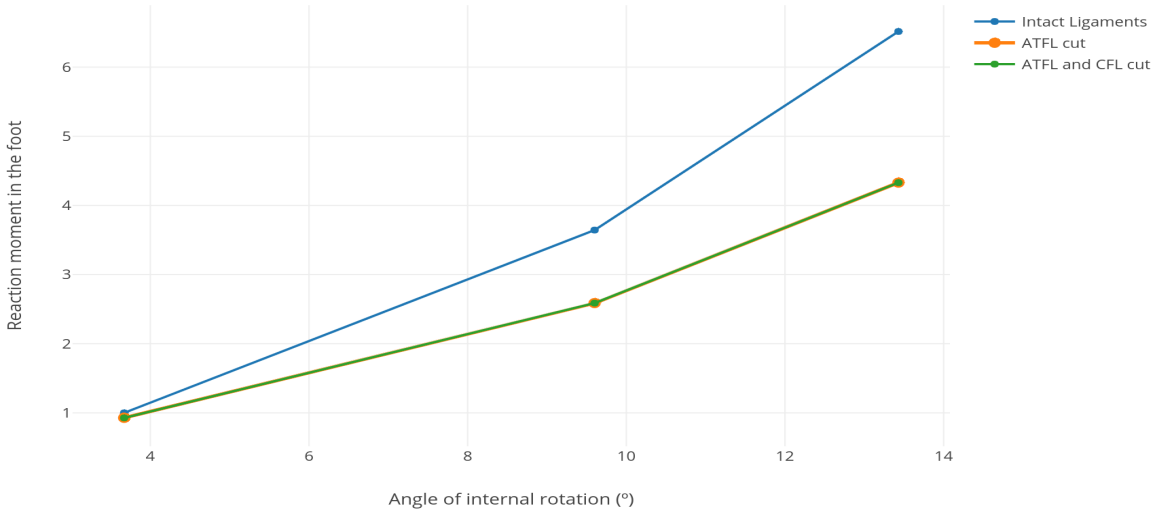

Figure 4.6: Values for the normalized reaction moments in the foot, for IRs of 3.64°, 9.6°and 13.43°and for the model with intact ligaments - blue trace - with ATFL cut - orange trace - and ATFL and CFL cut - green line.

13.43°. The values for both the ATFL cut and a combination of ATFL and CFL cut are equal. For the same 3.67°of IR, both the models with the ATFL cut and ATFL and CFL cut produce a smaller reaction moment than the model with the intact ligaments. For both of these models, the reaction moments for 9.6°and 13.43°are 2.58 and 4.32 times higher than the reaction moment for the intact ligaments and 3.67°of IR. To summarize, using the same rotation angle, the reaction moment decreases with the cut of the ATFL, staying the same with the cut of the CFL. Additionally, considering the same ligamentous configuration, the reaction moment raises with the increasing of the IR angle.

4.4.2 Discussion

The analysis and understanding of the reaction moments as a function of not only the IR angle, but also of the ligamentous configuration is important to assess ligamentous function and ankle instability. In fact, Cawley et al. [87] evaluated the effects of axial loads and single plane motions on ligament strain patterns and measured IR reaction torques for an intact ankle with and without the presence of an axial load - 650 N - and for all the possible ankle movements - DF, PF, inversion, eversion, IR and external rotation. Cadaveric feet were attached to a force platform and strain transducers were attached to the ATFL and to the CFL. Focusing on the IR tested, an angle of 15°was applied to an neutral ankle, and the values of the torque were of 5.7±5.06 N m for the IR without an axial load and of 9.7±4.2 N m with the presence of an axial load.

Although in the FE model a compressive axial force of 10 N is applied and the maximum rotational angle applied is not the same, considering the value of the reaction moment for an angle of IR of 13.43°applied in an intact ligamentous configuration, the value of 8.93 still falls into the range of values of the first case described by Cawley et al. without an axial load. It is also stated by Cawley et al. that the presence of an axial load leads to an higher reaction moment due to the fact that surface contact provides an increased resistance to IR. This happens due to the anatomy of both the talus and the tibial articular cages, which force some degree of external rotation, straining even more the ATFL. This data is particularly important for rehabilitation of injured ligaments, since by knowing the effects of the ankle position and of the axial load on ligament strain and ankle reaction torque, rehabilitation protocols can

be improved, as well as the development of new orthotic devices.

Six years before, Stormont et al. [88] established the percentage change in torque with sectioning of lateral ligaments, by using cadaveric ankles and applying inversion, eversion, IR and external rotation for a neutral ankle, a 20°plantar flexed ankle and a 20°dorsiflexed ankle. Comparing the percentage change in torque obtained for an IR after the sectioning of the ATFL measured by Stormont et al. - 7% -, and the difference between the normalized reaction moments for the intact ligaments and after the cut of the ATFL for an angle of 3.67°, the values support the hypothesis that for a neutrally placed ankle, the contribution of the ATFL is higher when compared with the contribution of, for example, the PTTL. This happens since for the same IR angle, the ATFL has a higher strain and the reaction moment increases quicker when the ATFL is modelled than when it is cut. Stormont et al. postulated then that the IR for a neutral ankle without any kind of loading has two main restraints, the ATFL and the PTTL, and that under loading, the articular surface becomes as important as the ligament restraint, when it comes to ankle stability [88].

The reaction moments measured are an important tool to understand the main restraints of ankle stability, with the ATFL and the PTTL being two of the most important ligaments in the control of ankle IR, and the articular surface as a third restraint, even more for a loaded ankle and after ligamentous injury. This third restraint is a valuable information to understand the cartilaginous injury mechanism after ligamentar rupture.

Chapter 5

Conclusion

The main focus of this thesis was to analyze the contact pressure patterns on the ankle cartilage after ligamentar lesion. This was done by modelling the AJ using a CT scan and a segmentation software, ITK SNAP®. After the segmentation of each bone, namely tibia, fibula, talus, calcaneus, navicular and cuboid, the 3D solid models were generated in SolidWorks®, along with the cartilages, and imported to ABAQUS®. The most relevant ligaments were then defined using medical descriptions and other existing FE models of the ankle. Considering the work done by Guerra-Pinto et al., it was possible to understand not only the *in vivo* exclusive rotational behavior of the AJ under biological conditions and after ligamentar rupture, but also the importance of the LCL in the IR. The magnitude of the IR as well as the ligamentous configuration described by their work were used as basis for the simulations developed in this thesis, namely the rotation of 3.67°for the intact ligamentar configuration, the rotation of 9.6°after the cut of the ATFL and the rotation of 13.43°after the cut of both the ATFL and the CFL. A 10 N axial force was also included in the model to ensure cartilaginous contact.

This work determined the contact patterns for the 3 situations described. The results showed not only an increase in the maximum pressure in the 3 cartilages - talar, tibial, and fibular, but also is notorious the occurrence of anteromedial and posterolateral spots of pressure. These spots of pressure can be directly connected to cartilage degeneration and are a computational evidence that links the LCL injury to pathological cartilaginous pressures. In particular, the maximum pressures rised from 3.11 MPa to 4.77 MPa in the talar cartilage, from 3.09 MPa to 4.75 MPa in the tibial cartilage and from 2.23 MPa to 3.63 MPa in the fibular cartilage. To the author's knowledge, no documented values of contact pressure are described in the literature. However, the peak stresses on the talar cartilage were also extracted from the FE model and compared with the literature, showing that in this model a submaximal stress is observed in the cartilage. This submaximal stress can, nevertheless, induce cartilaginous injury through a cycled loading of the cartilage surface, as it has been documented by Brand [82]. However one of the main limitations of this work is that the axial load applied in the ankle joint is only used to accommodate the cartilaginous surfaces and cannot be considered as biological. Hence, every stress or pressure noted in the cartilage is likely to be submaximal when compared to other works that use biological loadings. The results taken from the FE model can, nonetheless, be a starting point to the understanding of cartilage damage in unstable ankles.

The ligamentous strains were also analyzed in this work to understand the importance of the ligamentar structure not only in the control of the foot, but also to evaluate the influence on the cartilaginous pressures measured. In fact, it was perceived that both the ATFL and the PTTL had high strains when compared with the other ligaments. This ligamentar activation follows what is present in the available literature, only having differences in the CFL strains. This ligament is thought to have little importance in the IR, but still having some degree of strain. However, in this work, the CFL shortens, denoting that

either the orientation of the ligament could not be the ideal or that the movement of the ankle could also have some degree of abduction - which is known to shorten the CFL.

Lastly, the reaction moments were evaluated and compared to the ones present in the literature, with the values extracted from the FE model growing with the increase of the rotation magnitude and lowering with the cut of the ATFL since this ligament opposes the IR. The lack of strain of the CFL explains the same reaction moment for the same angle for the last two ligamentar configurations considered. By comparing the values retrieved from the FE model for the reaction moments with the literature available, it can be noticed that both the ATFL and the PTTL are the two main restraints to IR, highly influencing the reaction moment of the ankle. The articular cartilage is also an important restraint, possibly explaining why the damage is higher after ligamentar injury.

It is important to mention that, to the authors knowledge, this is the only FE study in the literature that focuses on ankle rotation, meaning that this thesis can be a basis for future research on rotational instability and cartilaginous injury. The weaknesses of this study are discussed in the next section and, if addressed properly, can help on the better understanding of the rotational behavior of the ankle.

5.1 Limitations and Future Work

To the authors knowledge, this work is the first to consider the ankle's rotational instability and evaluate the cartilage pressure patterns for the situation of an healthy ankle and for the situation of an unhealthy ankle. This thesis can then be the starting point for the further study of pathological movements of the ankle, namely rotational movements. The model has, nevertheless, some limitations which should be addressed to create a more outright representation of the ankle, thus being able to better represent and reproduce the *in vivo* conditions.

The first limitation has to do with the mechanical properties used in this work. Bone, cartilage and ligaments were modelled as linear elastic, isotropic and homogeneous, when in fact they possess other characteristics. Although almost all bones were considered as rigid bodies in this study, further studies should abandon that constraint and include a differentiation between cortical bone and trabecular bone. In terms of cartilage, since it is the main objective of the study, it should be modelled as close to reality, assuming a viscoelastic law [18]. The same should be done for ligaments assuming also anisotropic and viscoelastic material properties [89].

One other limitation is related to the ligament definition. As seen in the results section, the model is sensitive to the ligament positioning and orientation, meaning that changes in that orientation or attachment site can induce a new set of final results, namely in the ligamentous strains and reaction moments. Due to this, a proposed approach would be either to do a sensitivity analysis to the ligaments or to model them with more than one truss - which would be a better approach to ligamentous modelling since ligaments are composed of multiple collagenous fibers and not of one single fiber [17].

Lastly, it is relevant to mention that the main axis was defined through qualitative criteria and could have a high influence in ligamentous strains - such as the strains measured in the CFL which did not verify the literature. Due to this, it would be important to determine more accurately the exact position of the MA.

To conclude, further investigation is required and could follow the limitations described above and, after the dissection of the rotational instability, other movements could be analyzed. Some guidelines are presented:

- Perform a sensitivity analysis to the MA and evaluate its importance to the ankle ligament's strains and to the contact pressure of the ankle cartilage.
- Modelling of the cartilage as a viscoelastic material.

- Modelling of the ligaments with a higher number of fibers and with viscoelastic law.
- Analyze the cartilage pressure and ligamentous strains for every day movements such as gait cycle in the case of ligamentar chronic injury.
- Study cartilage pressure patterns for a multiplanar movement in the case of ligamentar injury.

References

[1] M. Kimizuka, H. Kurosawa, and T. Fukubayashi, "Load-bearing pattern of the ankle joint. Contact area and pressure distribution.," *Archives of orthopaedic and trauma surgery*, vol. 96, no. 1, pp. 45–49, 1980.

[2] P. A. Houglum and D. B. Bertoti, *Brunnstorm's Clinical Kinesiology*. F.A. Davis, 6 ed., 2012.

[3] D. T. P. Fong, Y. Hong, L. K. Chan, P. S. H. Yung, and K. M. Chan, "A systematic review on ankle injury and ankle sprain in sports," *Sports Medicine*, vol. 37, no. 1, pp. 73–94, 2007.

[4] S. L. Haddad, "Sprained Ankle," 2016.

[5] F. Guerra-Pinto, N. Côrte-Real, T. Mota Gomes, M. D. Silva, J. G. Consciência, M. Monzo, and X. M. Oliva, "Rotational Instability after Anterior Talofibular and Calcaneofibular Ligament Section: The Experimental Basis for the Ankle Pivot Test," *Journal of Foot and Ankle Surgery*, 2018.

[6] C. L. Saltzman, M. L. Salamon, G. M. Blanchard, T. Huff, A. Hayes, J. a. Buckwalter, and A. Amendola, "Epidemiology of ankle arthritis: report of a consecutive series of 639 patients from a tertiary orthopaedic center.," *The Iowa orthopaedic journal*, vol. 25, pp. 44–6, 2005.

[7] Phone, "Osteoporosis and Arthritis: Two Common but Different Conditions," *Bone*, no. April, pp. 202–223, 2015.

[8] K. D. Harrington, "Degenerative arthritis of the ankle secondary to long-standing lateral ligament instability.," *The Journal of Bone & Joint Surgery*, vol. 61, pp. 354–361, 4 1979.

[9] P. E. Scranton, J. E. Mcdarmott, and J. V. Rogers, "The Relationship between Chronic Ankfe Instability and Variations in Mortise Anatomy and ImpEngement Spurs," *Orthopedics*, vol. 21, pp. 657–664, 2000.

[10] I. Taga, K. Shino, M. Inoue, K. Nakata, A. Maeda, and J. H. Henry, "Articular cartilage lesions in ankles with lateral ligament injury. An arthroscopic study," *American Journal of Sports Medicine*, vol. 21, pp. 120–127, 1 1993.

[11] S. J. Hall, *Basic Biomechanics. 6th Edition*. New York: McGraw-Hill, 6th ed., 2012.

[12] M. Nordin and V. H. Frankel, "Basic Biomechanics of the Musculoskeletal System," in *New York* (D. Leger and A. Lis, eds.), ch. 9, pp. 222– 255, New York: Lippincott Williams & Wilkins, 3rd ed.

[13] C. L. Brockett and G. J. Chapman, "Biomechanics of the ankle," *Orthopaedics and Trauma*, vol. 30, no. 3, pp. 232–238, 2016.

[14] G. Tortora and B. Derrickson, *Principles of Anatory and Physiology*. 2010.

[15] Magee, "Orthopedic Assessment," *Igarss 2014*, pp. 1–5, 2014.

[16] I. Logics, “Insole Logics,” 2017.

[17] R. Drake, W. Vogl, and A. Mitchell, *Gray’s Anatomy for Students*. 2009.

[18] L. A. Setton, D. M. Elliott, and V. C. Mow, “Altered mechanics of cartilage with osteoarthritis: Human osteoarthritis and an experimental model of joint degeneration,” *Osteoarthritis and Cartilage*, vol. 7, no. 1, pp. 2–14, 1999.

[19] J. P. Arokoski, J. S. Jurvelin, U. Väätäinen, and H. J. Helminen, “Normal and pathological adaptations of articular cartilage to joint loading,” *Scandinavian Journal of Medicine and Science in Sports*, vol. 10, no. 4, pp. 186–198, 2000.

[20] G. Musumeci, “The Effect of Mechanical Loading on Articular Cartilage,” *Journal of Functional Morphology and Kinesiology*, vol. 1, no. 2, pp. 154–161, 2016.

[21] H. Zwipp and T. Randt, “Ankle joint biomechanics,” *Foot and Ankle Surgery*, vol. 1, no. 1, pp. 21–27, 1994.

[22] M. Bouysset, *Bone and Joint Disorders of the Foot and Ankle: A Rheumatological Approach*. 2013.

[23] A. S.Kelikian and S. K. Sarrafian, *Sarrafian’s Anatomy of the Foot and Ankle: Descriptive, Topographic, Functional*. 3rd ed., 2011.

[24] B. Manaster, J. Crim, and Z. S. Rosenberg, *Diagnostic and Surgical Imaging Anatomy*. Salt Lake City: Amirsys, 1st ed., 2007.

[25] W. Platzer, *Color Atlas of Human Anatomy, vol1: Locomotor System*. Stuttgart: Thieme, 7th ed., 2004.

[26] L. M. Ross, E. D. Lamperti, M. Schuenke, E. Schulte, and U. Schumacher, *Thieme Atlas of Anatomy: General Anatomy and Musculoskeletal System*. Stuttgart: Thieme, 2010.

[27] M. Rodgers, “Dynamic Foot Biomechanics,” *Journal of Orthopaedic and Sports Physical Therapy*, vol. 21, no. 6, pp. 306–316, 1995.

[28] A. K. Singh, K. D. Starkweather, A. M. Hollister, S. Jatana, and A. G. Lupichuk, “Kinematics of the ankle: A hinge axis model,” *Foot and Ankle*, vol. 13, no. 8, pp. 439–446, 1992.

[29] J. Goodsir, *The Anatomical memoirs of John Goodsir vol. II*, vol. XXX. 1859.

[30] R. Fick, *Handbuch der Anatomie und Mechanik der Gelenke*. Leipzig: Jena, 1st ed., 1904.

[31] R. Isman and V. Inman, “Anthropometric Studies of the Human Foot and Ankle,” *Foot Ankle*, vol. 11, pp. 97–129, 1969.

[32] J. Sammarco, “Biomechanics of the ankle: I. Surface velocity and instant center of rotation in the sagittal plane,” *The American Journal of Sports Medicine*, vol. 5, no. 6, pp. 231–234, 1977.

[33] C. Barnett and J. Napier, “The axis of rotation at the ankle joint in man. Its influence upon the form of the talus and the mobility of the fibula.,” *Journal of Anatomy*, vol. 86, no. 1, pp. 1–9, 1952.

[34] J. Hicks, “THE MECHANICS OF THE FOOT, IV.,” *Cells Tissues Organs*, vol. 27, no. 3, pp. 180–192, 1956.

[35] A. Lundberg, O. K. Svensson, and G. Nemeth, “The axis of rotation of the ankle joint,” tech. rep., 1989.

[36] A. Lundberg, I. Goldi, B. Kalin, and G. Selvik, “Kinematics of the ankle/foot complex-Part 1: Plantarflexion and dorsiflexion,” *Foot and Ankle*, vol. 9, no. 4, pp. 194–200, 1989.

[37] A. Lundberg, O. K. Svensson, C. Bylund, I. Goldie, and G. Selvik, “Kinematics of the Ankel/Foot Complex - Part 2: Pronation and Supination,” *Foot and Ankle*, vol. 9, no. 5, pp. 248–253, 1989.

[38] A. Lundberg, O. K. Svensson, C. Bylund, and G. Selvik, “Kinematics of the ankle/foot complex. Part 3: Influence of leg rotation,” *Foot and Ankle*, vol. 9, no. 6, pp. 304–309, 1989.

[39] A. J. van den Bogert, G. D. Smith, and B. M. Nigg, “In vivo determination of the anatomical axes of the ankle joint complex: An optimization approach,” *Journal of Biomechanics*, vol. 27, pp. 1477–1488, 12 1994.

[40] W. Thoma, D. Scale, and A. Kurth, “Computergestützte Analyse der Kinematik des oberen Sprunggelenks,” *Zeitschrift für Orthopädie und ihre Grenzgebiete*, vol. 131, pp. 14–17, 3 2008.

[41] A. Leardini, J. O’Connor, F. Catani, and S. Giannini, “A geometric model of the human ankle joint,” *Journal of Biomechanics*, vol. 32, no. 6, pp. 585–591, 1999.

[42] H. Zwipp, S. Rammelt, and R. Grass, “Ligamentous injuries about the ankle and subtalar joints,” *Clinics in Podiatric Medicine and Surgery*, vol. 19, no. 2, pp. 195–229, 2002.

[43] W. Petersen, I. V. Rembitzki, A. G. Koppenburg, A. Ellermann, C. Liebau, G. P. Brüggemann, and R. Best, “Treatment of acute ankle ligament injuries: A systematic review,” *Archives of Orthopaedic and Trauma Surgery*, vol. 133, no. 8, pp. 1129–1141, 2013.

[44] H. Tropp, “Commentary : Functional Ankle Instability Revisited,” vol. 37, no. 4, pp. 512–515, 2002.

[45] G. L. Lentell, L. L. Katzman, and M. R. Walters, “The Relationship Between Muscle Function and Ankle Stability,” *Journal of Orthopaedic & Sports Physical Therapy*, vol. 11, no. 12, pp. 605–611, 1990.

[46] J. Hertel, “Functional anatomy, pathomechanics, and pathophysiology of lateral ankle instability,” *Journal of Athletic Training*, vol. 37, no. 4, pp. 364–375, 2002.

[47] J. Hönigschmied, “Leichenexperimente über die Zerreissungen der Bänder im Sprunggelenk mit Rücksicht auf die Entstehung der indirecten Knöchelfracturen,” *Deutsche Zeitschrift für Chirurgie*, no. 2-3, pp. 239–260, 1877.

[48] H. Zwipp, R. Hoffmann, H. Thermann, and B. W. Wippermann, “Rupture of the ankle ligaments,” *International Orthopaedics*, vol. 15, no. 3, pp. 245–249, 1991.

[49] C. N. Van Dijk, B. W. J. Mol, L. S. Lim, R. K. Marti, and P. M. Bossuyt, “Diagnosis of ligament rupture of the ankle joint: Physical examination, arthrography, stress radiography and sonography compared in 160 patients after inversion trauma,” *Acta Orthopaedica*, vol. 67, no. 6, pp. 566–570, 1996.

[50] H. Polzer, K. G. Kanz, W. C. Prall, F. Haasters, B. Ockert, W. Mutschler, and S. Grote, “Diagnosis and treatment of acute ankle injuries: development of an evidence-based algorithm,” *Orthopedic Reviews*, vol. 4, no. 1, p. 5, 2011.

[51] S. Nakamura, R. D. Crowninshield, and R. R. Cooper, “An analysis of soft tissue loading in the Foot — A preliminary report,” *Bulletin of Prosthetics Research*, vol. 18, no. 1, pp. 27–34, 1981.

[52] K. M. Patil, L. H. Braak, and A. Huson, “Stresses in a simplified two dimensional model of a normal foot - A preliminary analysis,” *Mechanics Research Communications*, vol. 20, no. 1, pp. 1–7, 1993.

[53] S. Jacob, K. M. Patil, L. H. Braak, and A. Huson, “A three dimensional two arch model of a normal foot for stress analysis,” *Engineering*, pp. 23–24, 1995.

[54] Z. Xu-shu, G. U. O. Yuan, and C. Wei-yi, “3-D Finite Element Method Modeling and Contact Pressure Analysis of the Total Knee Joint in Flexion,” *In Vivo*, no. Nsfc 10702048, pp. 8–10, 2009.

[55] A. Gefen, M. Megido-Ravid, Y. Itzchak, and M. Arcan, “Biomechanical Analysis of the Three-Dimensional Foot Structure During Gait: A Basic Tool for Clinical Applications,” *Journal of Biomechanical Engineering*, vol. 122, no. 6, p. 630, 2000.

[56] J. T.-m. Cheung, M. Zhang, A. K.-l. Leung, and Y.-b. Fan, “Three-dimensional finite element analysis of the foot during standing — a material sensitivity study,” vol. 38, pp. 1045–1054, 2005.

[57] C. Dyrby, L. B. Chou, T. P. Andriacchi, and R. A. Mann, “Functional Evaluation of the Scandinavian Total Ankle Replacement,” *Foot & Ankle International*, vol. 25, no. 6, pp. 377–381, 2004.

[58] P. L. R. Wood, H. Prem, and C. Sutton, “Total ankle replacement: MEDIUM-TERM RESULTS IN 200 SCANDINAVIAN TOTAL ANKLE REPLACEMENTS,” *Journal of Bone and Joint Surgery - British Volume*, vol. 90-B, no. 5, pp. 605–609, 2008.

[59] M. Ozen, O. Sayman, and H. Havitcioglu, “Modeling and stress analyses of a normal foot-ankle and a prosthetic foot-ankle complex,” *Acta of Bioengineering and Biomechanics*, vol. 15, no. 3, pp. 19–27, 2013.

[60] D. S. Rodrigues, *Biomechanics of the Total Ankle Arthroplasty : Stress Analysis and Bone Remodeling*. PhD thesis, Instituto Superior Técnico, 2013.

[61] F. Wei, D. T. P. Fong, K. M. Chan, and R. C. Haut, “Estimation of ligament strains and joint moments in the ankle during a supination sprain injury,” *Computer Methods in Biomechanics and Biomedical Engineering*, vol. 18, no. 3, pp. 243–248, 2015.

[62] C.-w. Wang, A. Muheremu, and J.-p. Bai, “Use of three-dimensional finite element models of the lateral ankle ligaments to evaluate three surgical techniques,” 2018.

[63] T. Golditz, S. Steib, K. Pfeifer, M. Uder, K. Gelse, R. Janka, F. F. Hennig, and G. H. Welsch, “Functional ankle instability as a risk factor for osteoarthritis: Using T2-mapping to analyze early cartilage degeneration in the ankle joint of young athletes,” *Osteoarthritis and Cartilage*, vol. 22, no. 10, pp. 1377–1385, 2014.

[64] M. R. Colville, R. A. Marder, J. J. Boyle, and B. Zarins, “Strain measurement in lateral ankle ligaments,” *The American Journal of Sports Medicine*, vol. 18, no. 2, pp. 196–200, 1990.

[65] J. N. Parker and P. M. Parker, *CT Scan: A Medical Dictionary, Bibliography, and Annotated Research Guide to Internet References*. San Diego, California: Health Care, 2003.

[66] N. S. Ribeiro, P. Fernandes, D. S. Lopes, J. Folgado, and P. R. Fernandes, “3-D solid and finite element modeling of biomechanical structures - a software pipeline,” *7th EUROMECH Solid Mechanics Conference*, no. OCTOBER, 2009.

[67] P. Cignoni, P. Cignoni, M. Callieri, M. Callieri, M. Corsini, M. Corsini, M. Dellepiane, M. Dellepiane, F. Ganovelli, F. Ganovelli, G. Ranzuglia, and G. Ranzuglia, “MeshLab: an Open-Source Mesh Processing Tool,” *Sixth Eurographics Italian Chapter Conference*, pp. 129–136, 2008.

[68] W. X. Niu, L. J. Wang, T. N. Feng, C. H. Jiang, Y. B. Fan, and M. Zhang, "Effects of bone Young ' s modulus on finite element analysis in the lateral ankle biomechanics," vol. 10, pp. 189–195, 2013.

[69] S. A. Millington, M. Grabner, R. Wozelka, D. D. Anderson, S. R. Hurwitz, and J. R. Crandall, "Quantification of ankle articular cartilage topography and thickness using a high resolution stereophotography system," *Osteoarthritis and Cartilage*, vol. 15, no. 2, pp. 205–211, 2007.

[70] O. Rasmussen, *Stability of the Ankle Joint*, vol. 56. 1985.

[71] F. Corazza, J. J. O'Connor, A. Leardini, and V. P. Castelli, "Ligament fibre recruitment and forces for the anterior drawer test at the human ankle joint," *Journal of Biomechanics*, vol. 36, no. 3, pp. 363–372, 2003.

[72] P. C. Liacouras and J. S. Wayne, "Computational Modeling to Predict Mechanical Function of Joints: Application to the Lower Leg With Simulation of Two Cadaver Studies," *Journal of Biomechanical Engineering*, vol. 129, no. 6, p. 811, 2007.

[73] J.-Y. Rho, L. Kuhn-Spearing, and P. Zioupos, "Mechanical properties and the hierarchical structure of bone," *Medical Engineering & Physics*, vol. 20, pp. 92–102, 3 1998.

[74] J. T.-m. Cheung and M. A. Zhang, "A 3-Dimensional Finite Element Model of the Human Foot and Ankle for Insole Design," vol. 86, no. February, 2005.

[75] S. Siegler, J. Block, and C. D. Schneck, "The mechanical characteristics of the collateral ligaments of the human ankle joint," *Foot & ankle*, vol. 8, no. 5, pp. 234–242, 1988.

[76] B. A. Hills and B. D. Buttler, "Surfactants identified in synovial fluid and their ability to act as boundary lubricants," *Annals of the Rheumatic Diseases*, vol. 43, no. 4, pp. 641–648, 1984.

[77] S. C. Tadepalli, A. Erdemir, and P. R. Cavanagh, "Comparison of hexahedral and tetrahedral elements in finite element analysis of the foot and footwear," *Journal of Biomechanics*, vol. 44, no. 12, pp. 2337–2343, 2011.

[78] G. Li, L. Wan, and M. Kozanek, "Determination of real-time in-vivo cartilage contact deformation in the ankle joint," *Journal of Biomechanics*, vol. 41, no. 1, pp. 128–136, 2008.

[79] L. Wan, R. J. de Asla, H. E. Rubash, and G. Li, "Determination of in-vivo articular cartilage contact areas of human talocrural joint under weightbearing conditions," *Osteoarthritis and Cartilage*, vol. 14, no. 12, pp. 1294–1301, 2006.

[80] K. Hirose, G. Murakami, T. Minowa, H. Kura, and T. Yamashita, "Lateral ligament injury of the ankle and associated articular cartilage degeneration in the talocrural joint: Anatomic study using elderly cadavers," *Journal of Orthopaedic Science*, vol. 9, no. 1, pp. 37–43, 2004.

[81] J. E. Bischof, C. E. Spritzer, A. M. Caputo, M. E. Easley, J. K. DeOrio, J. A. Nunley, and L. E. DeFrate, "In vivo cartilage contact strains in patients with lateral ankle instability," *Journal of Biomechanics*, vol. 43, no. 13, pp. 2561–2566, 2010.

[82] R. A. Brand, "Joint Contact Stress: a Reasonable Surrogate for Biological Processes?," *The Iowa Orthopaedic Journal*, vol. 25, pp. 82–94, 2005.

[83] A. J. Ting, R. R. Tarr, A. Sarmiento, K. Wagner, and C. Resnick, "The Role of Subtalar Motion and Ankle Contact Pressure Changes from Angular Deformities of the Tibia," *Foot & Ankle International*, vol. 7, no. 5, pp. 290–299, 1987.

[84] S. J. Steffensmeier, C. L. Saltzmann, K. S. Berbaum, and T. D. Brown, “Effects of medial and lateral displacement calcaneal osteotomies on tibiotalar joint contact stresses,” *Journal of Orthopaedic Research*, vol. 14, no. 6, pp. 980–985, 1996.

[85] J. H. Calhoun, F. li, B. R. Ledbetter, and S. F. Viegas, “A Comprehensive Study of Pressure Distribution in the Ankle Joint with Inversion and Eversion,” *Foot & Ankle International*, vol. 15, no. 3, pp. 125–133, 1994.

[86] E. Dehne, “Die Klinik der frischen und habituellen Adduktionssupinationsdistorsion des Füßes,” *Langenbeck’s Archives of Surgery*, vol. 242, no. 1, pp. 40–60, 1933.

[87] P. W. Cawley and E. P. France, “Biomechanics of the lateral ligaments of the ankle: An evaluation of the effects of axial load and single plane motions on ligament strain patterns,” *Foot and Ankle*, vol. 12, no. 2, pp. 92–99, 1991.

[88] D. M. Stormont, B. F. Morrey, K. N. an, and J. R. Cass, “Stability of the loaded ankle:Relation between articular restraint and primary and secondary static restraints,” *The American Journal of Sports Medicine*, vol. 13, no. 5, pp. 295–300, 1985.

[89] C. Bonifasi-Lista, S. P. Lake, M. S. Small, and J. A. Weiss, “Viscoelastic properties of the human medial collateral ligament under longitudinal, transverse and shear loading.,” *Journal of orthopaedic research : official publication of the Orthopaedic Research Society*, vol. 23, no. 1, pp. 67–76, 2005.

Appendix A

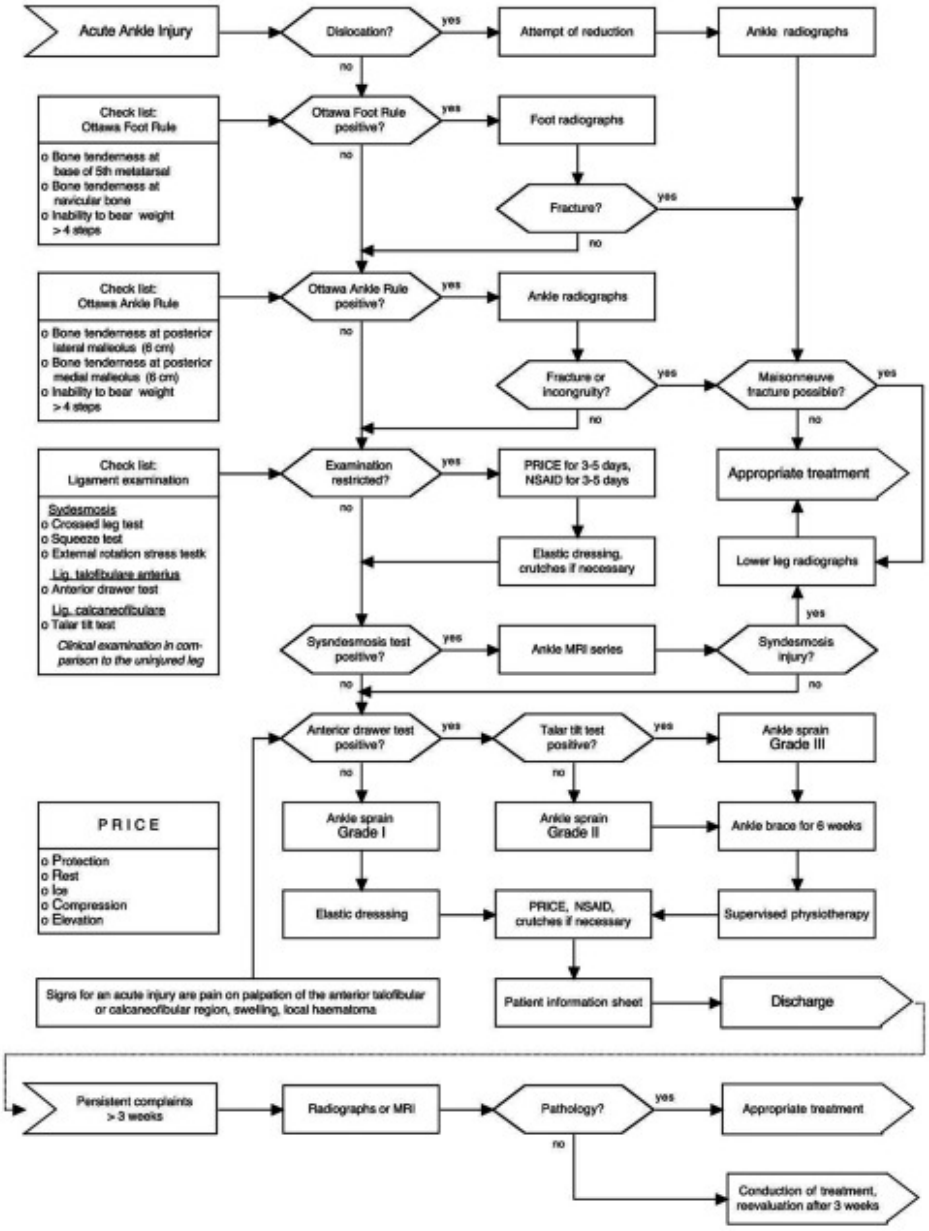

Figure A.1: Acute ankle injury diagnosis algorithm. Adapted from [50]

Table A.1: Equivalent stresses for the talar tilt test for a normal ankle and after 3 different LCL reconstruction techniques. Retrieved from Wang et al. [62]

Group	Equivalent stress of ATFL (MPa)	Equivalent stress of CFL (MPa)	Equivalent stress of peroneus longus tendon (MPa)	Equivalent stress of peroneus brevis tendon (MPa)
Normal	138.48	25.90	3.44	2.40
One-half peroneus longus tendon reconstruction	119.05	33.25	8.90	4.96
One-half peroneus brevis tendon reconstruction	118.82	32.64	8.10	2.94
Allogeneic tendon reconstruction	84.00	27.01	3.95	2.45

Table A.2: Equivalent stresses for the anterior drawer test for a normal ankle and after 3 different LCL reconstruction techniques. Retrieved from Wang et al. [62]

Group	Equivalent stress of ATFL (MPa)	Equivalent stress of CFL (MPa)	Equivalent stress of peroneus longus tendon (MPa)	Equivalent stress of peroneus brevis tendon (MPa)
Normal	61.67	69.83	20.63	26.75
One-half peroneus longus tendon reconstruction	31.31	28.60	16.05	40.94
One-half peroneus brevis tendon reconstruction	31.47	29.07	23.13	32.89
Allogeneic tendon reconstruction	57.32	52.20	21.71	38.03

Table A.3: Values of maximum pressure (MPa) for the 7 cases analyzed by Kimizuka et al [1] and for the FE analysis.

	500 N	1000 N	1500 N
Case 2	4	6	8
Case 3	9	10	12
Case 4	5	8	11
Case 5	4	8	13
Case 6	4	7	8
Case 7	2	5	9
Case 8	3	6	8
FE Method	6.239	7.865	9.637

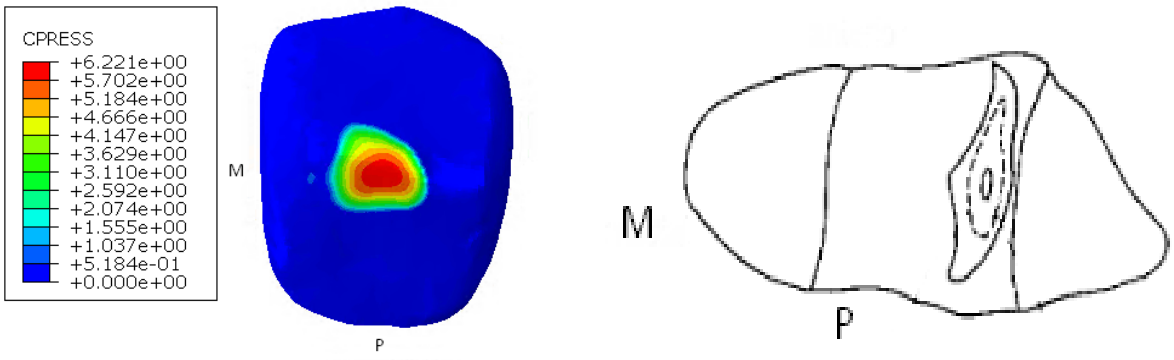

(a) (b)

Figure A.2: (a) FE model of the talar cartilage with the contact pressure values for the 500 N compressive load. The maximum contact pressure is in red and corresponds to 6.239 MPa and the medial and posterior orientations are marked with a ”M” and ”P” respectively. (b) *In vivo* pattern of pressure distribution taken from the work done by Kimizuka et al [1].

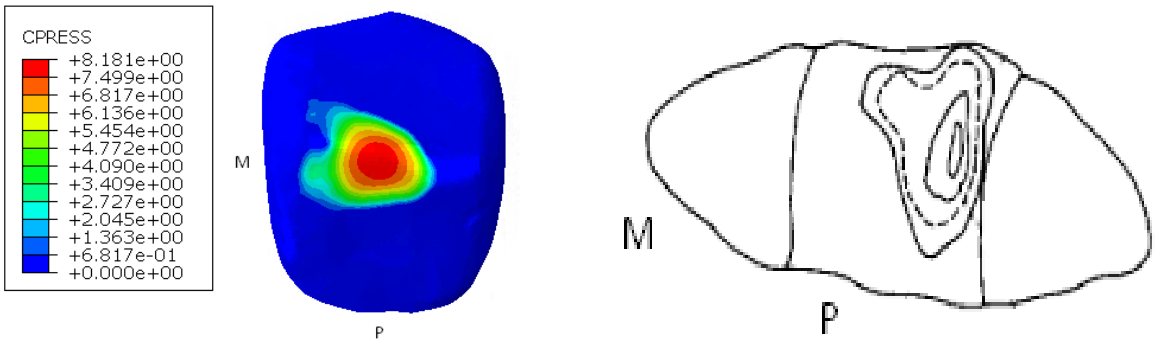

(a) (b)

Figure A.3: (a) FE model of the talar cartilage with the contact pressure values for the 1000 N compressive load. The maximum contact pressure is in red and corresponds to 7.865 MPa and the medial and posterior orientations are marked with a ”M” and ”P” respectively. (b) *In vivo* pattern of pressure distribution taken from the work done by Kimizuka et al [1].